

## Energy Minimization of Crystal Structures Containing Flexible Molecules

Panagiotis G. Karamertzanis and Sarah L. Price\*

*Department of Chemistry, University College London, 20 Gordon Street,  
London, United Kingdom WC1H 0AJ*

Received March 24, 2006

**Abstract:** This paper proposes a new methodology for the accurate minimization of crystal structures of flexible molecules. The intramolecular contributions to the crystal energy are calculated from ab initio calculations and appear well-balanced with the intermolecular interactions being evaluated via a conformation-dependent distributed multipole model in conjunction with an empirical repulsion–dispersion potential model. The validity of the methodology was initially tested by minimizing the experimental crystal structures of a set of flexible molecules. In a more stringent test, the methodology was used to refine the low-energy structures found in rigid-body crystal structure prediction studies of the diastereomeric salt pair (*R*)-1-phenylethylammonium (*R/S*)-2-phenylpropanoate and the antiepileptic drug carbamazepine. The refinement improved the relative stability of the known forms and their ranking in the list of hypothetically generated structures by leading to energetically more favorable hydrogen-bond geometries and dispersion interactions.

### 1. Introduction

Most crystal structure prediction algorithms rely on the generation of a large number of hypothetical crystal structures and their subsequent energy minimization based on some force field.<sup>1</sup> Recent crystal structure prediction blind tests<sup>2–4</sup> organized by the Cambridge Crystallographic Data Centre revealed that, for a limited number of crystallographically independent molecules and conformational degrees of freedom, the experimentally determined polymorphs usually appear somewhere in the list of putative low-energy structures. Thus, with the exceptions of flexible molecules, complicated asymmetric units,<sup>5,6</sup> and the occurrence of a rare space group, the problem seems to be not the search methodology but the selection of a few stable structures from the multitude of minima<sup>7</sup> with sufficiently close packing arrangements. A critical comparative study of all participants' submissions<sup>8</sup> in the latest blind test for crystal structure prediction<sup>4</sup> showed that the energy models used in the modeling of the organic solid state are not yet sufficiently reliable for this task.

The exact energy ranking of the putative structures, and consequently the success of the prediction, depends on the force-field parametrization. When the energy penalty involved in a structurally significant change in molecular conformation is comparable to the improvement this can produce in the binding energy of a molecular cluster, the force field needs to contain terms for both intra- and intermolecular contributions. The accuracy of the intermolecular potential can be greatly improved by modeling the electrostatic interactions with distributed multipoles derived directly from the wave function.<sup>9,10</sup> For rigid molecules, the use of distributed multipoles<sup>9,11,12</sup> offers a significant improvement in the reproduction of hydrogen-bonded crystals and the ranking of hypothetical crystal structures<sup>13</sup> in comparison with atomic charge models. However, in the case of flexible molecules, the benefits of realistic anisotropic intermolecular energy models are diminished when the latter are combined with empirical intramolecular force fields, which often lead to nonphysical distortion of the molecular geometry that prevents the accurate reproduction of the known crystal structures<sup>14</sup> and their favorable ranking with respect to hypothetical structures.<sup>15</sup> This failure can be attributed to the inaccurate force-field parametrization, as

\* Corresponding author tel.: +44 (0)20 7679 4622; fax +44 (0)-20 7679 7463; e-mail: s.l.price@ucl.ac.uk.

the inter- and intramolecular models are often derived separately and thus there is no guarantee that they will be sufficiently well-balanced to model the deformations of the molecular structure caused by the packing forces within the crystal.<sup>16</sup>

Poor accuracy often arises from various assumptions associated with the desire to achieve a compromise between accuracy on one side and computational cost and ease of implementation on the other. The charge distribution is only approximately transferable between different conformations due to local effects and the through-space polarization when the rotation around single bonds alters the relative positions of polar and polarizable parts of the molecule.<sup>17–19</sup> Thus, it is often not sufficient to fix the multipoles in their local axes system for modeling molecular clusters<sup>20</sup> and crystal structures.<sup>14</sup> Thus, the ab initio recalculation of the electrostatic model following any significant conformational change is necessary.<sup>21,22</sup> Fortunately, electronic structure calculations can provide both the intermolecular electrostatic model and the deformation energy from the gas-phase optimal geometry, avoiding the inaccuracies of empirical intramolecular force fields. Although computationally expensive, this approach has successfully been applied in crystal structure prediction studies for glycol,<sup>23</sup> glycerol,<sup>23</sup> and a series of six monosaccharides.<sup>24</sup>

This paper describes a hybrid computational methodology for the accurate lattice energy minimization of flexible molecules by combining a realistic electrostatic model for the intermolecular interactions based on distributed multipoles with ab initio intramolecular energies. The approach implemented in the program DMAflex extends the applicability of the hybrid approach originally applied by van Eijck et al.<sup>23,24</sup> to alcohols by considering a wider range of functional groups. The accuracy of the methodology is first assessed by its ability to reproduce (section 3) the lattice geometric parameters and conformational degrees of freedom for a set of experimentally determined crystal structures (Tables 1 and 2). Some of these crystal structures were chosen because they were poorly reproduced in a previous investigation of the ability of an empirical force field to model the crystal structures of flexible organic molecules of pharmaceutical complexity.<sup>14</sup>

The usefulness of the methodology in crystal structure prediction is investigated by refining the hypothetical crystal structures generated earlier by rigid-body search methodologies, to assess the effect of packing-induced molecular distortions on their relative stability (section 3.2). The systems considered (Table 2) are the diastereomeric salt pair (*R*)-1-phenylethylammonium (*R/S*)-2-phenylpropanoate, which exhibited significant sensitivity of the lattice energy to the ions' conformations,<sup>25</sup> and the antiepileptic drug carbamazepine for which spectroscopic and theoretical investigations indicate that a rigid model<sup>26</sup> may not be sufficient for reliable crystal structure prediction. The reranking of the putative crystal structures due to the packing-induced molecular distortions is shown to make a significant difference to the realism of the predictions.

## 2. Computational Methodology

Crystal structure prediction is generally based on the assumption that the experimentally determined polymorphs correspond to local minima in the crystal energy surface  $E^{\text{crys}}$ , which is usually partitioned into an intramolecular,  $\Delta E^{\text{intra}}$ , and an intermolecular,  $U^{\text{inter}}$ , energy contribution:

$$E^{\text{crys}} \equiv \Delta E^{\text{intra}}(\boldsymbol{\theta}) + U^{\text{inter}}(\mathbf{X}, \boldsymbol{\theta}) \quad (1)$$

with  $\Delta E^{\text{intra}}$  being the energy increase due to the deformation of the in vacuo molecular geometries in the crystalline solid.  $\mathbf{X}$  denotes the degrees of freedom that define the intermolecular contacts (referred to as lattice variables hereafter) for given molecular conformations, that is, lattice lengths, lattice angles, and the position and Euler angles for each of the  $M$  crystallographically independent molecular entities. For space groups other than triclinic, the presence of symmetry relations reduces the dimensionality of vector  $\mathbf{X}$ . The vector  $\boldsymbol{\theta}$  denotes the set of intramolecular degrees of freedom, that is,  $\sum_{j=1}^M (3N_j - 6)$  bond lengths, bond angles, and torsion angles, where  $N_j$  is the number of atoms for the molecular entity  $j$ .

The minimization of the crystal energy for flexible molecules is technically challenging because of the difficulties associated with the calculation of its derivatives with respect to the intramolecular degrees of freedom, as the multipole moments are an unknown function of the latter. However, the derivatives of the crystal energy with respect to the lattice variables  $\mathbf{X}$  have been computed analytically and implemented in rigid-body lattice modeling packages such as DMAREL.<sup>27</sup> A feasible way to exploit the availability of these analytical gradients is to reformulate the crystal energy minimization as a bilevel optimization problem:

$$\min_{\boldsymbol{\theta}} [\Delta E^{\text{intra}}(\boldsymbol{\theta}) + \min_{\mathbf{X}} U^{\text{inter}}(\mathbf{X}; \boldsymbol{\theta})] \quad (2)$$

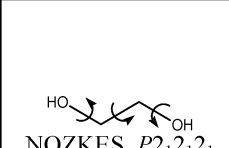
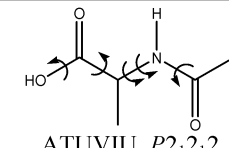
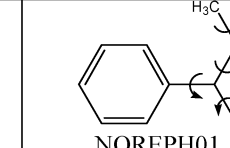
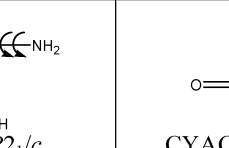
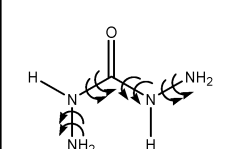
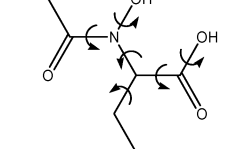
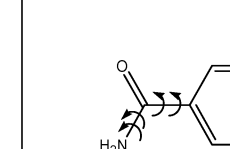
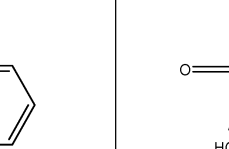
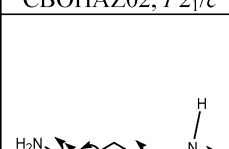
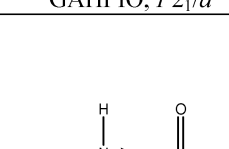

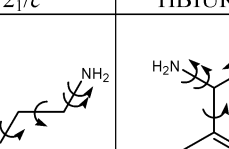

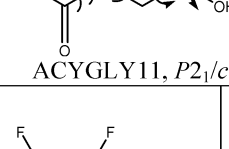

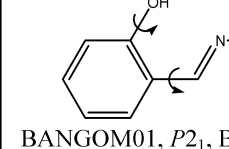
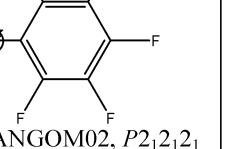

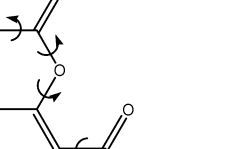
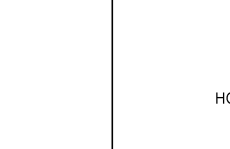
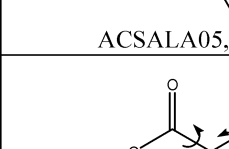
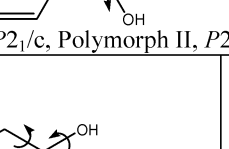
where the relative position and orientation of the molecular entities in the crystal are optimized at the inner minimization and the conformational degrees of freedom at the outer.

In molecular crystals, the intermolecular bonding energies are significantly weaker than the energy of typical covalent energies, and thus, the packing-induced molecular distortions are often limited.<sup>28,29</sup> More importantly, the number  $F$  of intramolecular degrees of freedom that can deviate appreciably from their in vacuo values (referred to as flexible hereafter) is usually much smaller than the dimensionality of  $\boldsymbol{\theta}$ . Thus, an approximation to the minimization problem is

$$\min_{\boldsymbol{\theta}^f} \{ \Delta E^{\text{intra}}(\boldsymbol{\theta}^f) + \min_{\mathbf{X}} U^{\text{inter}}[\mathbf{X}; \boldsymbol{\theta}(\boldsymbol{\theta}^f)] \} \quad (3)$$

where  $\boldsymbol{\theta}^f$  is the set of flexible degrees of freedom, such as torsion around single bonds. Assuming one crystallographically independent molecular entity for notational brevity, the rigid degrees of freedom, such as bond lengths, defined as the complement set  $\boldsymbol{\theta}^r \equiv \boldsymbol{\theta} / \boldsymbol{\theta}^f$ , are optimized at each step of the outer minimization problem via a constrained ab initio

**Table 1.** Molecular Structures with the Flexible Intramolecular Degrees of Freedom That Were Optimized within the Crystal Energy Minimization Indicated<sup>a</sup>

 NOZKES, $P_{21}2_12_1$	 ATUVIU, $P_{21}2_12$	 NOREPH01, $P_{21}/c$	 CYACHZ01, $P_{21}/c$
 CBOHAZ02, $P_{21}/c$	 GAHP10, $P_{21}/a$	 BZAMID02, $P_{21}/c$	 HBIURT10, $P_{21}2_12_1$
 HISTAN, $P_{21}$	 ACYGLY11, $P_{21}/c$	 KAYTUZ, $P_{21}/c$	 HUYYOP, $P_{21}2_12_1$
 BANGOM01, $P_{21}$ , BANGOM02, $P_{21}2_12_1$	 CENRIW, $P_{21}/n$	 HAMTIZ, $P_{21}/n$	
 ACSALA05, $P_{21}/c$ , Polymorph II, $P_{21}/c$	 IBPRAC01, $P_{21}/c$ , JEKNOC11, $P_{21}$ , $Z'=2$		
 EYOBAB, $Cc$	 KAMREW, $P_{21}2_12_1$	 PEAMAN01, $P_{21}$	
 LEKROI, $P_1$	 LEKRIC, $P_{21}2_12_1$		

<sup>a</sup> CSD reference codes given for the lowest temperature/lowest R-factor structures with preference to neutron determinations ( $Z'$  shown when greater than 1). Double arrows indicate the independent rotation of two fragments around the same single bond [for example, for KAYTUZ, both torsions C(Ph)–C(Ph)–N–C and C(Ph)–C(Ph)–N–H were considered flexible].

optimization that also provides the molecular deformation energy:

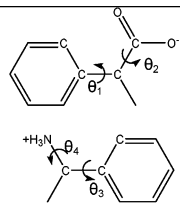
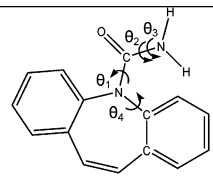
$$\theta^r(\theta^f) = \arg \min_{\theta^r} E^{\text{intra}}(\theta^f, \theta^r)$$

$$\Delta E^{\text{intra}}(\theta^f) = \min_{\theta^r} E^{\text{intra}}(\theta^f, \theta^r) - E^{\text{vac}} \quad (4)$$

where  $E^{\text{vac}}$  is the global minimum in vacuo molecular energy. This constant only needs to be computed once to compare the crystal energy to the experimentally determined heat of sublimation.<sup>30,31</sup>

The inner optimization problem in eq 3 is solved with the rigid-body crystal structure modeling program DMAREL.<sup>27</sup>

**Table 2.** Molecular Structures and CSD Reference Codes for the Known Polymorphs of (*R*)-1-Phenylethylammonium-(*R/S*)-2-phenylpropanoate<sup>a</sup> (left) and Carbamazepine<sup>a</sup> (right) for Which DMAflex Has Been Used for the Refinement of Putative Rigid-Body Crystal Structures in Addition to the Experimentally Determined Polymorphs

 <p>p-salt, <i>P</i>2<sub>1</sub> (PMACEP0x, reference 50) n-salt form I, <i>P</i>2<sub>1</sub>2<sub>1</sub>2<sub>1</sub> (NMACEP02) n-salt form II, <i>P</i>2<sub>1</sub>2<sub>1</sub>2<sub>1</sub> (NMACEP01)</p>	 <p>form I, <i>P</i>-1, <i>Z'</i>=4, (CBMZPN11) form II, <i>R</i>-3, (CBMZPN03) form III, <i>P</i>2<sub>1</sub>/<i>n</i>, (CBMZPN10) form IV, <i>C</i>2/<i>c</i>, (CBMZPN12)</p>
--	---

<sup>a</sup> The set of flexible torsions, defined by the explicitly labeled atoms, comprise the rotation of the phenyl  $\theta_1$  and  $\theta_3$ , carboxylate  $\theta_2$ , and ammonium  $\theta_4$  groups for 1-phenylethylammonium-2-phenylpropanoate and the rotation of the carboxamide group  $\theta_1$ , the independent rotation of the two amide hydrogen atoms  $\theta_2$  and  $\theta_3$ , and the torsion angle  $\theta_4$  defining the tilting of the carboxamide group with respect to the seven-member ring for carbamazepine.

For all of the results reported in this paper, the electrostatic interaction model comprises atomic multipoles up to hexadecapole,<sup>32</sup> derived through a distributed multipole analysis<sup>9,10,32</sup> of the molecular charge density computed at the MP2/6-31G(d,p) level of theory for the isolated molecule. The multipoles are computed each time the inner minimization problem is solved for the corresponding molecular geometry  $\theta$  to account for their conformational dependence. As one of the aims of this paper is to assess the reranking of the results of rigid-body searches due to conformational relaxation, we employed the same repulsion–dispersion potential. Thus, the repulsion–dispersion interactions were modeled with an empirical exp-6 potential with the parameters for the atomic types C, N, O, F, and H<sub>C</sub> (hydrogen connected to carbon) taken from Williams et al.<sup>33–35</sup> and for H<sub>N,O</sub> (hydrogen connected to nitrogen or oxygen) from a reparametrization of this force field in conjunction with atomic multipoles.<sup>12</sup> The contributions from the slowly convergent charge–charge, charge–dipole, and dipole–dipole interactions were accurately summed with the Ewald summation<sup>36</sup> technique, while higher multipole and repulsion–dispersion contributions were evaluated in direct space. Because quadrupole–charge interactions are only conditionally convergent (their distance dependence is  $R^{-3}$ ), a cutoff distance of 60.0 Å between the molecular centers of mass was used, which ensured that oscillations in lattice energy due to molecules coming in and out of the cutoff region<sup>37</sup> were sufficiently small.

The outer minimization problem is solved with the downhill simplex algorithm.<sup>38</sup> The initial simplex comprises  $F + 1$  points; the elements of the first point are set equal to the flexible degrees of freedom in the starting crystal structure  $\theta_o^f$ , and the other  $F$  points are set equal to  $\theta_i^f = \theta_o^f + \lambda_i \mathbf{e}_i$ , where  $\mathbf{e}_i$  are unit vectors. The characteristic length scales  $\lambda_i$  should be inversely proportional to the sensitivity of the crystal energy to the corresponding degree of freedom. For

bond angles or torsion angles which exhibit large intramolecular gradients or that may significantly affect the geometry of structure-defining interactions (and hence the intermolecular lattice energy), the parameters  $\lambda_i$  should be smaller than those with weaker lattice energy gradients, such as the rotation of methyl groups with no intra- and intermolecular steric repulsions. Generally, smaller values are preferable, although this may increase the number of iterations because of expansion of the first few simplices, to avoid failure of the inner lattice energy minimization because of severe conformational changes that may lead to close intermolecular contacts or saddle points. For all of the minimizations reported in this paper, we only consider torsion angles around single bonds (and in one case carboxylate bond angles, as explained in section 3.2.1) and set the length scale  $\lambda_i$  equal to 3° in all cases. A minimization is considered converged when the decrease in crystal energy in the terminating step is smaller than  $1 \times 10^{-4} E^{\text{cryst}}$ . For the systems discussed in this paper, this translates to a numerical accuracy in crystal energy of approximately 0.01–0.05 kJ mol<sup>-1</sup> depending on whether the crystal is molecular or ionic. For some crystals, the flexible degrees of freedom could only be converged to 1–2°, because of crystal energy oscillations on the order of a few tenths of a kilojoule per mole. This proved to result from minor discontinuities of the multipole moments with conformation generated by the distributed analysis method, as explained in the discussion.

The intramolecular energy and the rigid degrees of freedom are computed as a function of the flexible degrees of freedom at each iteration of the outer minimization by solving the optimization problem of eq 4 using the Gaussian<sup>39</sup> suite of programs. For all test cases considered, this optimization problem was first solved at the SCF/6-31G-(d,p) level of theory. To investigate the effect of electron correlation, a subset of the crystal structures was also modeled by using a second-order Møller–Plesset perturbation expansion with the same basis set. At each outer minimization iteration, the new molecular conformation obtained by solving the minimization problem (eq 4) needs to be inserted in the lattice. This is achieved by a least-squares overlap of the non-hydrogen atoms in the new molecular conformation and the one found in the crystal structure that had the lowest crystal energy in all previous outer minimization steps.

The methodology is first validated by the minimization of 32 experimentally determined crystal structures (section 3) reported for the 24 compounds shown in Tables 1 and 2. These crystal structures were retrieved from the Cambridge Structural Database (CSD)<sup>40</sup> by searching for good-quality determinations of both neutral and ionic compounds having a diverse variety of functional groups and degrees of flexibility, ranging from 3 to 16 flexible degrees of freedom. The sample includes some crystal structures previously modeled with an empirical intramolecular force field<sup>14</sup> (BANGCOM01, CENRIW, BANGCOM02, ACSALA05, IBPRAC01, JEKNOC11, PEAMAN01, LEKROI, and LEKRIC), where in several cases the molecular conformations significantly deformed from the experimental on energy minimization. The atom types were restricted to carbon,



oxygen, nitrogen, hydrogen, and fluorine, for which the parametrization of the repulsion–dispersion potential<sup>12,33–35</sup> has been extensively tested.

The accuracy of reproduction of the crystal structures was assessed on the basis of the root-mean-square ( $\text{RMS}_{15}$ ) deviation of a 15-molecule coordination sphere between the experimental and minimized crystal structures<sup>41</sup> (hydrogen atoms omitted in the comparison) and the errors in the reproduction of the conformational degrees of freedom, density, and lattice lengths and angles. The hydrogen atoms were not included in the comparison because of the apparent foreshortening of X–H bond lengths in their X-ray determinations. The modeling accuracy for the hydrogen atom positions can be more reliably established by the reproduction of the torsion angles involving hydrogen atoms, which are reported separately from other conformational degrees of freedom, and should be deduced in the light of X-ray limitations. To ensure that the occurrence of poor reproduction is not due to inaccuracies in the intermolecular potential, the structures were also minimized with the molecular geometries held rigid at their experimental conformations (Expt), with the hydrogen positions of the X-ray structures adjusted to standard neutron bond lengths.<sup>42</sup> A second rigid-body minimization was performed with the molecular conformations replaced with the ab initio optimized ones with the flexible degrees of freedom constrained to their experimental values (ConOpt). The  $\text{RMS}_{15}$  value for a ConOpt minimization also includes the effect of any minor deviations in the rigid degrees of freedom due to errors in their ab initio and experimental determinations or genuine deformations by the packing forces. A DMAflex refinement is considered successful if it leads to only a small increase in  $\text{RMS}_{15}$  compared with the ConOpt minimization.

### 3. Results

**3.1. Ability to Reproduce Known Crystal Structures as Energy Minima.** The errors in lattice lengths and angles and conformational degrees of freedom from the DMAflex minimization of the experimentally determined crystal forms are shown in Table 3. Although there is significant variation in the quality of reproduction, there are no cases for which the minimization leads to excessive distortions of the molecular conformations or unit cell geometries. This agreement with the experimental structures constitutes a substantial improvement over the previous study, which employed atomic multipole moments with empirical intramolecular force fields.<sup>14</sup> When the intramolecular energies are modeled at the HF/6-31G(d,p) level of theory, the average  $\text{RMS}_{15}$  discrepancy for the 32 structures considered is only 0.222 Å, which is generally within the uncertainties in energy minimization due to the neglect of thermal effects.

The accuracy of the crystal structure reproductions with DMAflex are not significantly worse than the reproductions with the molecular geometry fixed at the experimental conformation. The 31 Expt rigid-body minimizations had an average  $\text{RMS}_{15}$  error of 0.171 Å (Table 3) and, hence, demonstrate that the errors in the intermolecular force field are not significant. This success can be partially attributed to the use of distributed multipoles, which ensures the

accurate modeling of hydrogen-bonded systems.<sup>11,43</sup> The worst reproduction was observed in the case of KAYTUZ ( $\text{RMS}_{15} = 0.476$  Å), as the nitrogen–nitrogen distance of the hydrogen-bonded amide groups was overestimated with this model potential by 0.4 Å. Another case where the intermolecular potential is less accurate and gives rise to the worst DMAflex reproduction is that of HUYYOP, where the unusually elongated  $\text{NH}\cdots\text{H}$  distance (3.25 Å predominantly along the *a* crystallographic axis) is severely underestimated.

The rigid-body minimization with the ab initio optimized conformations with the flexible torsion angles held at the experimental values (ConOpt) has an average  $\text{RMS}_{15}$  error of 0.188 Å (Table 3) at the HF/6-31G(d,p) level of theory, which is comparable to the rigid-body reproduction accuracy with the experimental conformations (Expt). This confirms that packing forces within the crystals may only appreciably affect the flexible degrees of freedom identified in Tables 1 and 2. The other, less deformable degrees of freedom, can generally be reasonably predicted by isolated molecule, ab initio calculations at a relatively modest level of theory, such as HF/6-31G(d,p). It is encouraging that the simultaneous relaxation of the flexible intramolecular degrees of freedom by DMAflex does not substantially deteriorate the quality of reproduction despite increasing the number of minimization variables.

As shown in Table 3, overall, DMAflex reproduces the molecular conformations in the known crystals very well with small errors in the flexible torsion angles ( $\Delta\theta$  and  $\Delta\theta_{\text{H}}$ ), including subtle details such as the pyramidalization of amino groups. For example, the significant pyramidalization of both amino groups in HUYYOP, due to the balance of hydrogen bonding,  $\text{N}-\text{H}\cdots\pi$ , and steric interactions, is accurately reproduced, despite the 0.4 Å underestimation of the *a* cell length. One case where errors in the molecular geometry lead to poor overall reproduction is CYACHZ01, where an overestimation of the  $(\text{N}\equiv)\text{C}-\text{C}-\text{C}-\text{N}$  angle leads to an elongation of the *a* cell length because of steric repulsion from the nitrile group protruding from the amide plane. For KAMREW, the accuracy in the modeling of the hydrogen-bonding motif depends strongly on the level of theory for the intramolecular energy. The MP2 model is satisfactory, whereas the SCF model gives a large error in the torsion angle for the 3-hydroxyl group, which forms a nonphysical, bifurcated intermolecular hydrogen bond to a tartrate carboxyl and an ammonium-butanol hydroxy oxygen acceptor.

With the exception of KAMREW, the inclusion of electron correlation on the intramolecular energy estimates has little effect on the reproduction of the crystal structures by DMAflex. For the 15 systems also studied at the MP2/6-31G(d,p) level, the average  $\text{RMS}_{15}$  error was 0.229 Å compared with 0.179 Å when electron correlation was neglected. This is primarily because the two methods produce somewhat different intramolecular energy surfaces. This is corroborated by the similarity of the ConOpt  $\text{RMS}_{15}$  values at the HF/6-31G(d,p) and MP2/6-31G(d,p) levels of theory indicating that the differences in the rigid degrees of freedom in the molecular structures are minimal. It is expected that the method used to evaluate the intramolecular energy contributions  $\Delta E^{\text{intra}}(\theta^f)$  will be more important (but less

**Table 3.** Reproduction of Crystal Structures by Simultaneous Optimization of the Flexible Torsion Angles and Lattice Variables Contrasted with Rigid-Body Minimizations Using Experimental Information for the Molecular Conformation

structure	intra-molecular energy <sup>a</sup>	flexible-molecule										rigid-body	
		conventional unit cell					$\Delta\theta^c$ (deg)		$\Delta\theta_H^d$ (deg)		RMS <sub>15</sub> <sup>e</sup> (Å)	RMS <sub>15</sub> (Å)	
		a(Å)	b(Å)	c(Å)	angles <sup>b</sup> (deg)	density (g cm <sup>-3</sup> )	max	mean	max	mean		ConOpt <sup>f</sup>	Expt <sup>g</sup>
NOZKES		5.013	6.915	9.271		1.283							
	HF	-1.76%	+0.35%	+1.55%		-0.16%	3.28	3.28	8.39	6.22	0.122	0.143	
	MP2	-1.48%	+0.61%	+0.74%		+0.16%	2.86	2.86	12.29	3.22	0.133	0.165	0.255
ATUVIU		10.388	11.545	5.743		1.265							
	HF	-0.99%	+2.12%	-0.17%		-0.95%	4.82	2.92	4.68	4.18	0.161	0.129	
	MP2	-1.27%	+1.86%	+0.49%		-1.11%	6.14	3.67	7.01	4.36	0.160	0.137	0.191
NOREPH01		12.507	8.771	8.130	$\beta$ 106.20	1.173							
	HF	-0.99%	-3.74%	+1.55%	-1.35	+2.64%	0.67	0.65	3.10	2.25	0.249	0.235	
	MP2	+0.56%	-3.69%	+0.87%	+0.11	+2.39%	0.29	0.23	3.96	2.81	0.253	0.220	0.166
CYACHZ01		7.247	8.678	7.855	$\beta$ 116.80	1.493							
	HF	+7.81%	-0.62%	-0.82%	+3.58	-2.61%	11.43	6.94	6.12	3.15	0.329	0.205	
	MP2	+10.56%	-0.09%	-1.73%	+4.11	-4.22%	16.99	8.68	3.69	2.36	0.436	0.201	0.151
CBOHAZ02		3.618	8.789	12.487	$\beta$ 106.43	1.571							
	HF	-1.27%	-4.65%	+1.35%	+4.32	+7.51%	7.13	4.35	4.23	2.43	0.242	0.210	
	MP2	-1.24%	-3.60%	+3.11%	+5.73	+5.54%	11.44	8.49	10.27	6.80	0.287	0.190	0.202
GAHPHO		14.003	5.425	10.495	$\beta$ 93.70	1.345							
	HF	+2.24%	+1.14%	-3.00%	-1.21	-0.37%	8.72	2.94	7.34	5.19	0.235	0.179	
	MP2	+3.71%	+0.94%	-3.88%	-3.17	-0.89%	9.99	5.41	15.49	9.23	0.331	0.223	0.085
BZAMIDO02		5.529	5.033	21.343	$\beta$ 88.73	1.355							
	HF	-2.06%	+0.54%	+3.68%	-1.25	-1.92%	1.30	1.30	5.01	2.69	0.194	0.229	
	MP2	-1.56%	+1.29%	+3.64%	-1.50	-3.10%	1.65	1.65	7.54	4.14	0.206	0.238	0.196
HBIURT10		10.868	11.698	3.603		1.727							
	HF	-0.02%	-2.40%	-2.14%		+4.69%	6.80	4.49	8.22	5.39	0.217	0.191	
	MP2	+0.85%	-2.80%	-2.00%		+4.11%	19.57	16.28	14.34	7.37	0.266	0.203	0.140
HISTAN		7.249	7.634	5.698	$\beta$ 104.96	1.212							
	HF	-2.47%	+0.17%	+0.61%	+0.19	+1.82%	4.12	2.18	10.88	8.09	0.131	0.138	
	MP2	-1.92%	+0.35%	+0.68%	+0.33	+1.07%	4.64	2.70	9.12	7.93	0.121	0.121	0.146
ACYGLY11		4.859	11.546	14.633	$\beta$ 138.29	1.424							
	HF	+0.40%	-1.76%	+3.94%	+0.81	-0.56%	3.00	1.00	0.00	0.00	0.207	0.209	
	MP2	-0.21%	-1.37%	+4.22%	+0.64	-1.26%	4.96	2.35	3.49	1.78	0.227	0.225	0.177
KAYTUZ		10.668	8.958	10.308	$\beta$ 115.75	1.356							
	HF	-0.16%	-2.00%	+5.72%	+3.54	-0.15%	4.13	2.73	7.54	5.05	0.321	0.215	0.476
HUYUOP		5.145	12.326	18.536		1.200							
	HF	-8.55%	+3.12%	+3.95%		+2.00%	6.82	2.48	2.19	1.42	0.499	0.404	0.321
BANGOM01		12.738	7.263	6.039	$\beta$ 98.15	1.724							
	HF	+0.60%	+2.64%	+1.49%	+0.75	-4.35%	3.72	2.92	1.29	1.29	0.280	0.375	0.269
BANGOM02		12.101	7.373	12.890	$\beta$ 95.89	1.667							
	HF	+1.14%	-1.82%	+1.18%	+1.57	-0.12%	3.03	1.88	4.49	4.49	0.251	0.204	0.149
CENRIW		24.215	6.981	6.147	$\beta$ 91.70	1.236							
	HF	-0.64%	+1.35%	-1.92%	-0.77	+1.21%	3.18	2.29	8.97	4.19	0.173	0.200	0.119
HAMTIZ		12.569	4.853	17.266	$\beta$ 99.16	1.528							
	HF	+1.38%	+1.06%	+1.28%	+0.46	-3.53%	3.11	1.36	3.89	2.75	0.119	0.125	0.093
ACSALA05		11.186	6.540	11.217	$\beta$ 96.07	1.466							
	HF	+2.52%	+0.83%	+0.97%	+0.38	-4.09%	1.43	0.91	9.74	5.97	0.135	0.145	
	MP2	+0.29%	+2.87%	+1.70%	+0.38	-4.57%	4.27	2.03	8.01	5.08	0.164	0.153	0.150
acetylsalicylic acid, polymorph II		12.095	6.491	11.323	$\beta$ 111.51	1.447							
	HF	+1.37%	+0.79%	+0.51%	-0.22	-2.76%	2.98	1.81	0.38	0.23	0.113	0.125	
	MP2	-0.47%	+2.94%	+1.54%	+0.67	-0.346%	7.22	3.31	6.27	3.20	0.190	0.132	0.105
IBPRAC01		14.397	7.818	10.506	$\beta$ 99.7	1.176							
	HF	+2.76%	0.72%	+0.11%	-0.71	-3.74%	4.93	3.65	0.37	0.37	0.192	0.186	0.150
JEKNOC11		12.456	8.036	13.533	$\beta$ 112.86	1.098							
	HF	-1.40%	+0.97%	-1.24%	-1.53	+0.55%	6.04	2.67	5.44	3.52	0.164	0.127	0.189
EYOBAY		7.537	15.035	11.662	$\beta$ 106.81	1.340							
	HF	+0.49%	+0.76%	-0.39%	+1.13	-0.22%	8.42	4.61	6.22	0.35	0.159	0.100	
	MP2	+0.77%	+0.82%	+0.36%	+1.18	-1.27%	7.25	3.96	5.26	1.92	0.166	0.128	0.079
KAMREW		7.296	9.484	16.020		1.433							
	HF	-4.43%	-1.83%	+2.80%		+3.70%	6.60	2.25	75.13	15.45	0.255	0.151	
	MP2	-2.47%	-1.52%	+1.82%		+2.30%	6.39	4.40	11.03	4.41	0.199	0.164	0.105
PEAMAN01		8.322	6.801	12.885	$\beta$ 91.74	1.245							
	HF	-1.26%	+2.19%	+0.82%	+2.66	-1.45%	11.86	7.92	13.39	7.06	0.256	0.176	
	MP2	-0.32%	+2.73%	+0.23%	+2.86	-2.25%	12.30	8.78	9.79	5.50	0.284	0.188	0.134
LEKROI					$\alpha$ 95.42								
					+0.44								
					$\beta$ 99.48								
	HF	+1.75%	+2.90%	-1.88%	-0.30	-2.51%	4.37	2.17	12.04	6.46	0.185	0.152	0.120
					$\gamma$ 108.99								
					+0.15								
LEKRIC		9.997	10.347	12.680		1.268							
	HF	+4.30%	-1.33%	-1.15%		-1.74%	8.08	3.95	14.06	8.16	0.209	0.169	0.209
Systems for Which Crystal Structure Prediction Was also Performed													
PMACEP0x (p-salt)		11.008	6.539	12.160	$\beta$ 116.01	1.146							
	HF	+0.35%	+0.95%	-1.07%	-0.22	-0.44%	9.77	7.67	5.01	5.01	0.234	0.164	0.190
NMACEP02 (n-salt form I)		5.797	15.444	17.073		1.179							
	HF	+5.26%	+1.06%	-4.26%		-1.78%	16.40	11.23	6.28	6.28	0.382	0.176	0.112
NMACEP02 (n-salt form II)		5.941	15.469	17.501		1.121							
	HF	+5.08%	+0.70%	-5.29%		-0.27%	9.92	7.69	4.42	4.42	0.349	0.283	0.200

Table 3. Continued

structure	intra-molecular energy <sup>a</sup>	flexible-molecule						rigid-body				
		conventional unit cell				$\Delta\theta^c$ (deg)		$\Delta\theta_H^d$ (deg)		RMS <sub>15</sub> <sup>e</sup> (Å)	RMS <sub>15</sub> (Å)	
		a(Å)	b(Å)	c(Å)	angles <sup>b</sup> (deg)	max	mean	max	mean		ConOpt <sup>f</sup>	Expt <sup>g</sup>
CBMZPN11 (form I)					$\alpha$ 84.12 +0.94 $\beta$ 88.01 −1.01 $\gamma$ 85.19 +0.94							
	HF	5.171 −1.20%	20.574 +1.02%	22.245 +1.81%		1.339 −1.87%	6.73 2.60	15.34 8.35		0.248	0.139	0.137
CBMZPN03 <sup>h</sup> (form II)	HF	35.454 +0.55%	35.454 +0.55%	5.253 −2.08%		1.235 +0.97%	1.34 0.81			0.113		
CBMZPN10 (form III)	HF	7.537 +1.87%	11.156 −0.37%	13.912 −1.70%	$\beta$ 92.86 −0.28	1.343 +0.22%	1.21 0.79	4.88 4.33		0.169	0.176	0.177
CBMZPN12 (form IV)	HF	26.609 +0.54%	6.927 +0.49%	13.957 +2.68%	$\beta$ 109.72 +1.55	1.233 +2.35%	0.60 0.48	4.98 4.12		0.198	0.183	0.122

<sup>a</sup> Intramolecular energies and molecular geometries were computed (eq 4) with the 6-31G(d,p) basis set at the HF and MP2 levels. <sup>b</sup> Only angles not determined by space group symmetry are given. <sup>c</sup> Maximum/average absolute change of non-hydrogen torsion angles during refinement. <sup>d</sup> Maximum/average absolute change of hydrogen torsion angles during refinement. <sup>e</sup> Root-mean-square overlap of the 15-molecule coordination sphere of the experimental and minimized structures for the flexible-molecule lattice energy minimization (DMAflex). <sup>f</sup> Root-mean-square overlap of the 15-molecule coordination sphere of the experimental and minimized structures for rigid-body lattice energy minimization with the ab initio optimized conformations with the flexible torsions frozen to their experimental values (ConOpt). <sup>g</sup> Root-mean-square overlap of the 15-molecule coordination sphere of the experimental and minimized structures for rigid-body lattice energy minimization with the experimental conformations and XH bond lengths adjusted to standard neutron values for X-ray determinations (Expt). <sup>h</sup> Hydrogen atom positions have not been experimentally determined.

practically feasible) for large molecules where the intramolecular dispersion between distant functional groups determines the intramolecular energy surface.<sup>44</sup>

In addition to reproducing the crystal and molecular structures, the DMAflex methodology should also provide realistic values for the energies and relative stabilities of known polymorphic forms. For the three polymorphic systems discussed in this section, aspirin form I (AC-SALA05) is predicted to be +0.18 kJ mol<sup>−1</sup> less stable than the metastable form II<sup>45</sup> (−0.08 kJ mol<sup>−1</sup> at the MP2 level), *n*-salicylidene-pentafluoroaniline form I (BANGOM01) is 2.20 kJ mol<sup>−1</sup> less stable than form II (BANGOM02), and the racemic form of the anti-inflammatory agent ibuprofen (IBPRAC01) is 5.93 kJ mol<sup>−1</sup> more stable than its stereoisomer (JEKNOC11). Although we are not aware of quantitative experimental relative stabilities for comparison, the predicted stability differences are plausible,<sup>46</sup> more so than earlier predictions with empirical force fields.<sup>14</sup> The crystal energies of the known forms of the polymorphic systems (*R*)-1-phenylethylammonium-(*R/S*)-2-phenylpropanoate and carbamazepine were also predicted to be within a few kilojoules per mole and will be discussed in the context of crystal structure prediction in the next section.

### 3.2. Reranking of Hypothetical Crystal Structures.

**3.2.1. Diastereomeric Salt Pairs: The Case of (*R*)-1-Phenylethylammonium (*R/S*)-2-phenylpropanoate.** The separation of enantiomeric pairs is a challenging and important aspect of the pharmaceutical and fine chemical industries,<sup>47</sup> as their physical properties are identical and, in most cases, crystallization produces racemic crystals.<sup>48</sup> A frequently used separation process relies on the addition of a carefully chosen optically pure resolving acid or base that will produce a diastereomeric salt pair with sufficiently different solubilities (free energies).<sup>49</sup> In a recent publication,<sup>25</sup> we reported a methodology for the crystal structure prediction of such systems by performing rigid-body searches for low-lattice-energy structures for the p-salt (*R,S*) and n-salt (*R,R*) of the diastereomeric salt pair system 1-phenylethyl-

ammonium-2-phenylpropanoate.<sup>25</sup> In these searches, the ion conformations had the torsion angles  $\theta_1$ ,  $\theta_2$ , and  $\theta_3$  (Table 2) constrained to values suggested by a statistical analysis of the CSD. The known p-salt structure<sup>50</sup> was predicted at the global minimum (columns 1 and 2 of Table 4). However, the thermodynamically stable form I of the n-salt<sup>51</sup> was ranked 12th and was 7.4 kJ mol<sup>−1</sup> less stable than the global conformational minimum, which corresponded to the metastable form II<sup>51</sup> (columns 1 and 2 of Table 5). Furthermore, it was predicted that the packing of p-salt structures is energetically favored by 11.6 kJ mol<sup>−1</sup> compared to that of n-salt structures, which does not agree with solution calorimetry measurements that suggest that the enthalpy of the p-salt is 3.9 kJ mol<sup>−1</sup> higher<sup>25</sup> than the enthalpy of the n-salt at 25 °C. Thus, although the search found all known forms within the low-energy region, the relative stability of the putative minima was not sufficiently accurate to assess the efficiency of (*R*)-1-phenylethylamine to resolve racemic 2-phenylpropanoic acid mixtures. In this section, we report the refinement of the rigid-body predictions for the 20 lowest-energy structures for each diastereomeric salt, by considering the effect of the packing forces on the most flexible degrees of freedom  $\theta_1$ ,  $\theta_2$ ,  $\theta_3$ , and  $\theta_4$  (Table 2) at the HF/6-31G-(d,p) level. These angles can vary by more than 40° with up to a 5 kJ mol<sup>−1</sup> increase in intramolecular energy.<sup>25</sup> The DMAflex refinement reproduces the three known enantiomorphous forms satisfactorily (Table 3), although the errors in lattice lengths are greater in the case of n-salt polymorphs. As demonstrated in the Supporting Information, further improvements in the reproduction accuracy will also require developments in the intermolecular potential, while small improvements are observed when the carboxylate angle is also included in the flexible degrees of freedom.

The refinement of the rigid-body putative structures considerably changes their relative energies, as shown in Figure 1 and Tables 4 and 5. In the case of the p-salt, the experimentally determined structure still corresponds to the global minimum, but for example, the 20th most stable

**Table 4.** Effect of Conformational Relaxation on the Relative Stability of (*R*)-1-Phenylethylammonium (*S*)-2-phenylpropanoate (p-salt) Putative Crystal Structures<sup>a</sup>

rigid-body search		flexible-ion refinement										
rank, space group	$U^b$ (kJ mol <sup>-1</sup> )	rank	$\Delta E^c$		$U^d + \Sigma \Delta E^c$ (kJ mol <sup>-1</sup> )	$\hat{V}^e$ (Å <sup>3</sup> )	anion			cation		
			anion	cation			RMS <sup>f</sup> (Å)	$\theta_1$ (deg)	$\theta_2$ (deg)	RMS <sup>f</sup> (Å)	$\theta_3$ (deg)	$\theta_4$ (deg)
<b>1, <i>P</i><sub>2</sub><sub>1</sub></b>	<b>-645.25</b>	<b>1</b>	<b>1.22</b>	<b>0.05</b>	<b>-655.00</b>	<b>394.95</b>	<b>0.118</b>	<b>-52.10</b> <b>(-61.87)</b>	<b>87.90</b> <b>(92.69)</b>	<b>0.030</b>	<b>75.00</b> <b>(66.56)</b>	<b>-64.84</b> <b>(-69.85)</b>
2, <i>P</i> <sub>2</sub> <sub>1</sub> <sub>2</sub> <sub>1</sub>	-642.61	3	2.45	1.12	-650.22	368.99	0.232	-63.18	84.97	0.201	61.84	-61.40
3, <i>P</i> <sub>2</sub> <sub>1</sub> <sub>2</sub> <sub>1</sub>	-636.89	10	4.28	0.98	-644.66	417.90	0.325	-69.40	89.07	0.151	66.85	-71.01
4, <i>C</i> <sub>2</sub>	-636.83	6	1.66	0.01	-647.82	416.34	0.129	-50.01	91.44	0.025	78.62	-62.65
5, <i>P</i> <sub>2</sub> <sub>1</sub> <sub>2</sub> <sub>1</sub>	-634.97	13	4.35	0.91	-641.24	430.90	0.308	-67.73	93.01	0.151	66.66	-70.21
6, <i>P</i> <sub>2</sub> <sub>1</sub> <sub>2</sub> <sub>1</sub>	-632.42	7	3.51	3.49	-647.17	413.47	0.310	-69.02	80.77	0.290	57.57	-78.62
7, <i>P</i> <sub>2</sub> <sub>1</sub> <sub>2</sub> <sub>1</sub>	-631.42	14	1.74	0.01	-641.07	430.03	0.132	-50.47	91.69	0.022	78.46	-62.71
8, <i>P</i> <sub>2</sub> <sub>1</sub> <sub>2</sub> <sub>1</sub>	-630.52	11	2.93	5.10	-643.38	402.43	0.192	-56.75	96.11	0.382	50.53	-78.85
9, <i>C</i> <sub>2</sub>	-630.40	9	2.43	5.86	-644.69	399.25	0.168	-54.56	94.50	0.438	45.53	-73.81
10, <i>C</i> <sub>2</sub>	-629.63	15	0.02	0.96	-639.98	427.20	0.014	-47.50	74.32	0.146	67.25	-71.17
11, <i>C</i> <sub>2</sub>	-628.26	4	1.88	0.01	-647.95	418.15	0.139	-51.28	92.49	0.018	75.50	-62.40
12, <i>P</i> <sub>2</sub> <sub>1</sub> <sub>2</sub> <sub>1</sub>	-628.03	8	4.30	5.21	-646.42	396.15	0.212	-44.51	103.63	0.404	48.32	-75.40
13, <i>C</i> <sub>2</sub>	-627.58	5	1.71	0.00	-647.86	417.19	0.131	-49.93	91.75	0.002	76.96	-62.66
14, <i>P</i> <sub>2</sub> <sub>1</sub> <sub>2</sub> <sub>1</sub>	-627.39	17	2.04	2.32	-638.24	411.04	0.196	-60.14	86.92	0.233	61.37	-75.66
15, <i>P</i> <sub>2</sub> <sub>1</sub> <sub>2</sub> <sub>1</sub>	-627.23	20	3.44	0.97	-633.99	391.84	0.280	-66.36	87.94	0.174	63.85	-60.26
16, <i>C</i> <sub>2</sub>	-627.18	19	7.05	0.45	-635.47	415.30	0.414	-73.57	104.82	0.128	67.44	-63.53
17, <i>P</i> <sub>2</sub> <sub>1</sub> <sub>2</sub> <sub>1</sub>	-626.69	12	4.73	1.24	-641.27	430.50	0.325	-68.74	94.18	0.181	64.52	-70.96
18, <i>C</i> <sub>2</sub>	-626.49	16	4.60	0.52	-639.77	373.32	0.378	-73.57	76.30	0.136	66.79	-62.43
19, <i>C</i> <sub>2</sub>	-626.14	18	1.54	0.02	-635.59	457.47	0.124	-56.55	82.07	0.029	71.64	-62.70
20, <i>P</i> <sub>2</sub> <sub>1</sub> <sub>2</sub> <sub>1</sub>	-625.46	2	0.71	0.68	-652.13	392.50	0.154	-35.28	71.14	0.132	67.88	-68.98

<sup>a</sup> The row in bold corresponds to the experimentally determined form with the experimental values of the intramolecular degrees of freedom shown in parentheses. <sup>b</sup> Where intermolecular lattice energy was calculated with a 15 Å cutoff distance for the repulsion–dispersion and higher multipole moment interactions; the rigid-body ion conformations were fixed at the MP2/6-31G(d,p) conformational minimum with the phenyl and carboxylate rotation constrained to the CSD average values and the atomic multipoles derived from the MP2/6-31G(d,p) charge density (ref 25). <sup>c</sup> HF/6-31G(d,p) intramolecular energy for the ion conformations at the crystal energy minimum. <sup>d</sup> Intermolecular lattice energy at the crystal lattice energy minimum with atomic multipoles derived from the MP2/6-31G(d,p) charge density and 60 Å cutoff distance for the repulsion–dispersion and higher multipole moment interactions; because of the differences in cutoff distance and level of theory for the determination of rigid degrees of freedom, the starting energies for the DMAflex refinement may differ from the energies in the second column by up to 5 kJ mol<sup>-1</sup>. <sup>e</sup> Cell volume per ion pair. <sup>f</sup> All-atom ion root-mean-square discrepancy from the HF/6-31G(d,p) global conformational minimum ( $\theta_1 = -46.84^\circ$ ,  $\theta_2 = 72.64^\circ$ ,  $\theta_3 = 76.82^\circ$ , and  $\theta_4 = -62.67^\circ$ ) due to the effect of the packing forces.

**Table 5.** Effect of Conformational Relaxation on the Relative Stability of (*R*)-1-Phenylethylammonium (*R*)-2-Phenylpropanoate (n-salt) Putative Crystal Structures

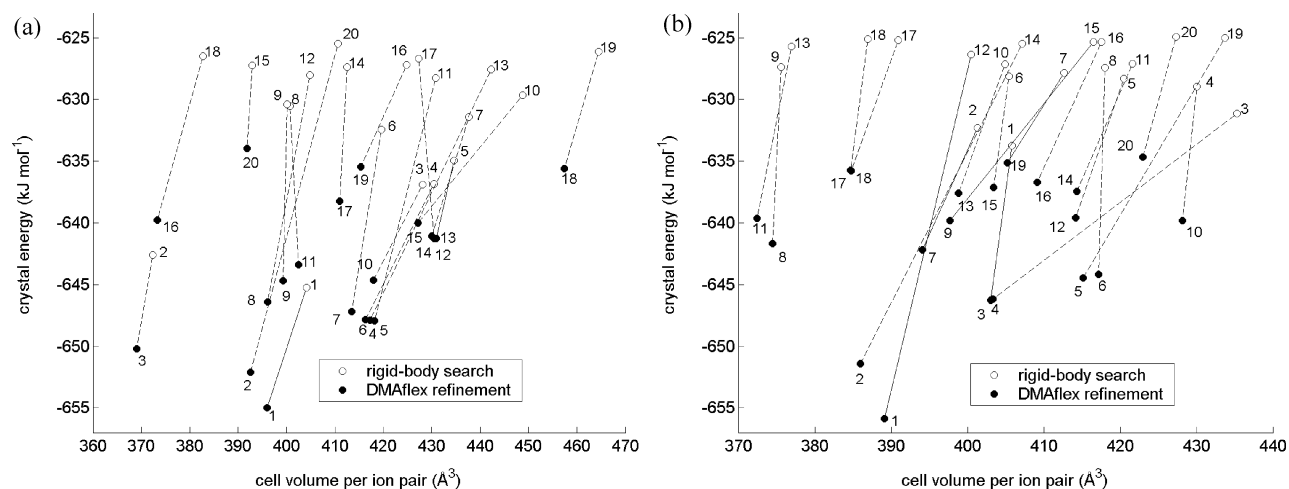
rigid-body search		flexible-ion refinement										
rank, space group	$U^b$ (kJ mol <sup>-1</sup> )	rank	$\Delta E^c$		$U^d + \Sigma \Delta E^c$ (kJ mol <sup>-1</sup> )	$\hat{V}^e$ (Å <sup>3</sup> )	anion			cation		
			anion	cation			RMS <sup>f</sup> (Å)	$\theta_1$ (deg)	$\theta_2$ (deg)	RMS <sup>f</sup> (Å)	$\theta_3$ (deg)	$\theta_4$ (deg)
<b>1, <i>P</i><sub>2</sub><sub>1</sub><sub>2</sub><sub>1</sub></b>	<b>-633.73</b>	<b>3</b>	<b>5.94</b>	<b>1.54</b>	<b>-646.25</b>	<b>403.04</b>	<b>0.389</b>	<b>72.86</b> <b>(76.26)</b>	<b>-97.14</b> <b>(-87.39)</b>	<b>0.166</b>	<b>66.54</b> <b>(56.62)</b>	<b>-74.92</b> <b>(-70.50)</b>
2, <i>P</i> <sub>2</sub> <sub>1</sub> <sub>2</sub> <sub>1</sub>	-632.30	7	2.18	3.49	-642.20	394.06	0.237	64.04	-79.09	0.333	52.55	-67.48
3, <i>P</i> <sub>2</sub> <sub>1</sub> <sub>2</sub> <sub>1</sub>	-631.13	4	5.76	1.71	-646.16	403.37	0.388	73.10	-95.07	0.165	67.02	-76.11
4, <i>P</i> <sub>2</sub> <sub>1</sub> <sub>2</sub> <sub>1</sub>	-628.95	10	0.91	0.79	-639.80	428.16	0.096	49.27	-86.37	0.142	67.20	-69.51
5, <i>P</i> <sub>2</sub> <sub>1</sub>	-628.31	12	1.94	2.14	-639.56	414.20	0.140	50.95	-92.93	0.195	64.90	-77.39
6, <i>P</i> <sub>2</sub> <sub>1</sub> <sub>2</sub> <sub>1</sub>	-628.11	15	3.05	1.65	-637.10	403.42	0.263	65.35	-86.48	0.230	60.09	-66.51
7, <i>P</i> <sub>2</sub> <sub>1</sub> <sub>2</sub> <sub>1</sub>	-627.84	19	4.92	0.93	-635.12	405.22	0.284	64.08	-101.28	0.173	64.53	-67.23
8, <i>P</i> <sub>2</sub> <sub>1</sub> <sub>2</sub> <sub>1</sub>	-627.43	6	0.44	0.59	-644.17	417.16	0.108	54.82	-74.94	0.171	89.46	-64.42
9, <i>P</i> <sub>2</sub> <sub>1</sub> <sub>2</sub> <sub>1</sub>	-627.38	8	3.77	1.93	-641.65	374.47	0.325	70.08	-80.34	0.167	64.92	-49.93
10, <i>P</i> <sub>2</sub> <sub>1</sub> <sub>2</sub> <sub>1</sub>	-627.16	13	2.30	0.00	-637.60	398.84	0.155	51.95	-94.77	0.004	76.60	-62.28
11, <i>C</i> <sub>2</sub>	-627.11	14	4.22	1.64	-637.45	414.32	0.341	70.95	-84.07	0.182	65.19	-74.63
<b>12, <i>P</i><sub>2</sub><sub>1</sub><sub>2</sub><sub>1</sub></b>	<b>-626.35</b>	<b>1</b>	<b>2.02</b>	<b>0.01</b>	<b>-655.88</b>	<b>389.15</b>	<b>0.222</b>	<b>59.80</b> <b>(71.13)</b>	<b>-56.88</b> <b>(-73.28)</b>	<b>0.021</b>	<b>75.25</b> <b>(69.28)</b>	<b>-62.36</b> <b>(-56.08)</b>
13, <i>P</i> <sub>2</sub> <sub>1</sub> <sub>2</sub> <sub>1</sub>	-625.70	11	0.40	1.21	-639.63	372.43	0.101	54.26	-75.82	0.196	62.79	-67.53
14, <i>P</i> <sub>2</sub> <sub>1</sub>	-625.50	2	0.24	1.43	-651.42	385.96	0.056	44.17	-65.93	0.191	63.89	-71.87
15, <i>P</i> <sub>2</sub> <sub>1</sub> <sub>2</sub> <sub>1</sub>	-625.36	9	7.54	0.35	-639.80	397.69	0.523	81.24	-102.82	0.106	68.98	-60.31
16, <i>P</i> <sub>2</sub> <sub>1</sub> <sub>2</sub> <sub>1</sub>	-625.35	16	5.63	2.12	-636.70	409.15	0.416	75.57	-88.33	0.169	64.94	-48.83
17, <i>P</i> <sub>2</sub> <sub>1</sub>	-625.20	17	1.16	1.12	-635.76	384.77	0.164	58.71	-79.81	0.181	64.18	-69.20
18, <i>P</i> <sub>2</sub> <sub>1</sub>	-625.13	18	1.24	1.13	-635.75	384.68	0.170	59.16	-79.79	0.183	64.02	-69.07
19, <i>P</i> <sub>2</sub> <sub>1</sub> <sub>2</sub> <sub>1</sub>	-625.03	5	0.32	0.35	-644.44	415.13	0.095	40.45	-76.50	0.107	69.30	-65.91
20, <i>P</i> <sub>2</sub> <sub>1</sub>	-624.90	20	3.82	2.83	-634.66	422.97	0.331	70.50	-78.86	0.275	58.00	-75.20

<sup>a</sup> The rows in bold correspond to the experimentally determined forms with the experimental values of the intramolecular degrees of freedom shown in parentheses. <sup>b–f</sup> As in Table 4.

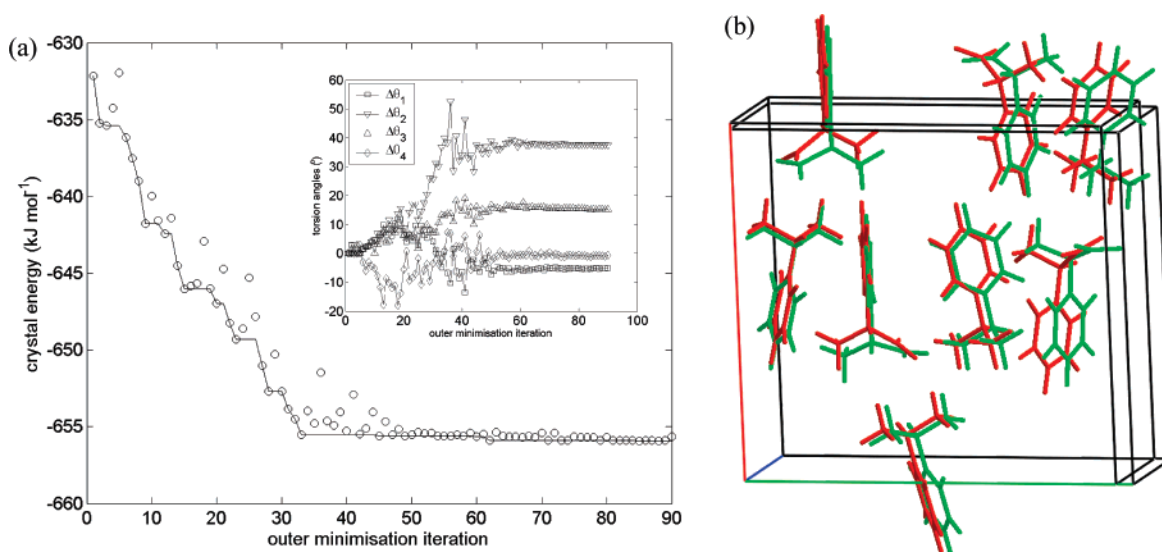
structure in the rigid-body search becomes the second, and its energy relative to the global minimum is reduced from 19.8 to 2.9 kJ mol<sup>-1</sup>. In the case of the n-salt, the changes in the ranking order are even more pronounced. The simultaneous relaxation of the intramolecular degrees of freedom brings the 12th most stable structure to the global minimum, which is in accord with experimental measure-

ments, as it corresponds to the thermodynamically stable polymorph. Furthermore, the metastable polymorph n-salt II becomes the third most stable structure, 9.6 kJ mol<sup>-1</sup> higher in energy. The second most stable minimum on the crystal energy surface, which was ranked 14th in the rigid-body search, has a distinct packing of the same hydrogen-bonding ladder as in the global minimum. The relaxation of





**Figure 1.** Refinement (full circles) of the 20 most stable crystal structures identified by the rigid-body search (open circles, ref 25) for the (a) p-salt and (b) n-salt of the diastereomeric salt pair (*R*)-1-phenylethylammonium (*R/S*)-2-phenylpropanoate. The solid lines correspond to experimentally determined polymorphs and the dashed lines to hypothetical low-energy crystal structures.



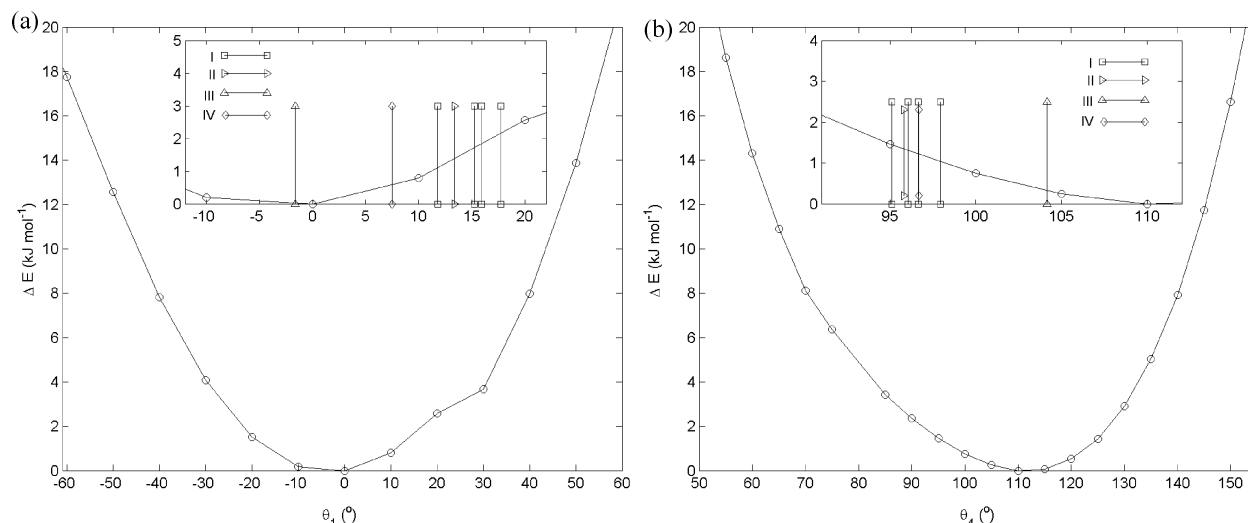
**Figure 2.** Simultaneous relaxation of the lattice variables and ion conformations starting at the 12th n-salt rigid-body minimum (corresponds to n-salt I polymorph). (a) The evolution of the crystal energy as a function of the outer minimization iteration (open circles; continuous line corresponds to the lowest-energy achieved up to the corresponding step). The inset illustrates the changes in the flexible torsion angles during refinement. (b) The overlay of the starting rigid-body structure (green) and flexible-ion lattice energy minimum (red).

the molecular geometries reduces the number of putative structures as some of the rigid-body minima lead to the same minimum. In the case of the n-salt, the global and third rigid-body minima differed by an  $\text{RMS}_{15}$  of  $0.73 \text{ \AA}$ , but the DMAflex refinement led to the same minimum, involving significant adjustments in the cell lengths and volume (Table 5). Similarly, the following clusters of rigid-body minima led to the same crystal energy minimum: n-salt 17th and 18th; p-salt 4th, 11th, and 13th; and p-salt 5th and 17th. In addition to the reduction of the number of putative structures, the simultaneous relaxation of the ion conformations increases the energy range for the 20 putative structures to  $21.0 \text{ kJ mol}^{-1}$  and  $21.2 \text{ kJ mol}^{-1}$  for the p-salt and n-salt, respectively, which leads to greater energetic separation between the known and hypothetical structures.

The simultaneous relaxation of the ion conformations also improves the calculated relative stability of the diastereomeric

salts. The thermodynamically most stable n-salt polymorph becomes  $0.9 \text{ kJ mol}^{-1}$  more stable than the p-salt structure, which is in reasonable agreement with the experimental value of  $3.9 \text{ kJ mol}^{-1}$  on the basis of solution calorimetry measurements.<sup>25</sup>

Figure 2 illustrates the changes that take place during a typical refinement for the rigid-body minimum corresponding to n-salt I polymorph. In accord with earlier observations regarding the significant sensitivity of the intermolecular lattice energy to the fine details of the ion conformations,<sup>25</sup> the crystal energy is reduced by approximately  $23 \text{ kJ mol}^{-1}$ , although the only significant change in conformation is in the rotation of the carboxylate group ( $\theta_2$ ), while the overall changes in the crystal structure are modest. Although the torsion angle changes for some structures in Tables 4 and 5 can exceed  $20^\circ$ , the average absolute changes for the torsion angles  $\theta_1$ ,  $\theta_2$ , and  $\theta_3$  during refinement are  $9.83^\circ$ ,  $10.07^\circ$ ,



**Figure 3.** One-dimensional intramolecular energy variation as a function of the (a) rotation  $\theta_1$  and (b) tilting  $\theta_4$  of the carboxamide group with respect to the seven-member ring at the B3LYP/6-31G(d,p) level of theory for carbamazepine. The conformational energy profiles were computed by constraining the scanning torsion and optimizing the rest of the molecular geometry. The insets show a magnification over the low-energy regions with the values corresponding to experimental conformations indicated. The discontinuity at  $\theta_1 = 30^\circ$  in part a is because the amine hydrogen atoms switch between two local minima (see Figure 4).

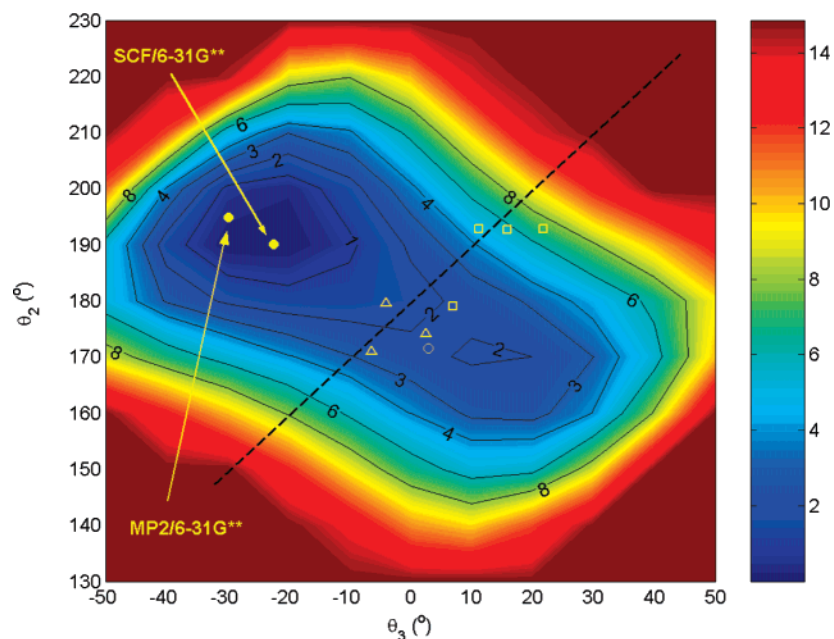
and  $8.62^\circ$ , respectively. The change in the ion torsion angles from the starting conformations appeared to be largely determined by the packing forces, as shown by the changes in the hydrogen-bonding geometries during the refinement (Tables S2 and S3 in Supporting Information) which approach their typical CSD values<sup>52–55</sup> for the majority of hypothetical structures. For example, the significant reranking of the structure corresponding to the n-salt I polymorph is associated with a  $0.15 \text{ \AA}$  reduction in the average  $\text{N}\cdots\text{O}$  distance, while the  $\text{H}\cdots\text{O}=\text{C}$  angle approaches its ideal value for all three hydrogen bonds to a single cation. Although the changes in ion conformation are mainly driven by the improvement in the hydrogen-bond geometries, there is also a dispersion contribution to the stabilization because most structures become denser, on average by 2%.

**3.2.2. Carbamazepine.** Extensive research on the solid state of carbamazepine (Table 2), a drug for the treatment of epilepsy and trigeminal neuralgia, has led to the crystallographic characterization of four polymorphs and several solvates and cocrystals.<sup>26,56–63</sup> A recent rigid-body crystal structure prediction study<sup>26</sup> [with the MP2/6-31G(d,p) optimized geometry] indicated that two energetically competitive  $\text{C}=\text{O}\cdots\text{N}-\text{H}$  hydrogen-bonding motifs [dimer  $R_2^2(8)$  and chain  $C(4)$  motifs] equally populate the set of low-energy minima. However, dimers are observed in all four polymorphs, solvates, and cocrystals. Whether the predicted stabilities of the hypothetical chain structures are artifacts of the rigid-body search<sup>26</sup> can be established by the DMAflex refinement of the most stable rigid-body putative crystal structures.

Carbamazepine comprises a rigid skeleton formed by two phenyl rings fused at the positions 3 and 4 of each side of a 5-azacycloheptene (azepine) ring, which appears conformationally locked in a boat configuration, as the angle between the two phenyl group planes varies little in the determined polymorphs (mean  $54.05^\circ$ , standard deviation  $2.02^\circ$ ) and ab initio optimized conformations [ $53.77^\circ$  and  $48.75^\circ$  for the

HF/6-31G(d,p) and B3LYP/6-31G(d,p) levels of theory, respectively]. However, the geometry of the pendant  $\text{CONH}_2$  group will be determined by the delicate balance of inter- and intramolecular forces. A recent spectroscopic study<sup>64</sup> revealed that the polymorph-sensitive IR modes are localized to the latter group and show the greatest disparity from the theoretical spectra, suggesting that the crystalline forces perturb its in vacuo geometry and relative position with respect to the carbamazepine backbone. A frequency analysis for an isolated molecule at the B3LYP/6-311\*\* $(2d,2p)$  level shows that the lowest and third vibrational modes at  $56.08 \text{ cm}^{-1}$  and  $85.35 \text{ cm}^{-1}$  predominately correspond to the tilting and rotation of the carboxamide group. A conformational analysis revealed that the rotation ( $\theta_1$ ) and tilting ( $\theta_4$ ) of the carboxamide group with respect to the seven-membered ring can both vary in a range of approximately  $50\text{--}60^\circ$  with less than a  $4 \text{ kJ mol}^{-1}$  increase in intramolecular energy, as shown by the relaxed scans at the B3LYP/6-31G(d,p) level in Figure 3. This agrees with an analysis of 16 carbamazepine solvates and cocrystals (CSD version 5.27, November 2005), in which  $\theta_1$  was found to vary in a range of  $22.1^\circ$  with an average value of  $9.8^\circ$ , while  $\theta_4$  varied across  $24.6^\circ$  with an average value of  $97.3^\circ$ . This shows a wider variation but the same systematic packing effect on the molecular conformation shown for the four polymorphs in the insets of Figure 3.

The set of flexible degrees of freedom should also include the independent rotation of the two amide hydrogen atoms,<sup>65</sup> which will affect the hydrogen-bond geometries and, hence, the relative stability of the hypothetical crystal structures. The intramolecular energy surface for the rotation of the amide hydrogen atoms at the B3LYP/6-31G(d,p) level exhibits two conformational minima: in the global minimum, the hydrogen atoms are pointing toward the seven-membered ring, whilst the second minimum is marginally less stable ( $1 \text{ kJ mol}^{-1}$ ) with the hydrogen atoms pointing in the opposite direction (Figure 4). All experimental structures with hydrogen atoms exhibit almost planar amide group geometries,



**Figure 4.** Two-dimensional intramolecular energy variation as a function of the independent rotation of the two amide hydrogen atoms (torsion angles  $\theta_2$  and  $\theta_3$ ) at the B3LYP/6-31G(d,p) level of theory for carbamazepine. The conformational energy surface was computed by constraining torsion angles  $\theta_2$  and  $\theta_3$  and optimizing the rest of the molecular conformation. Full circles correspond to ab initio global minima at different levels of theory, open triangles to the three determinations of the *P*-monoclinic polymorph (form III: CBMZPN10, CBMZPN01, and CBMZPN02), open squares to the four molecules present in the asymmetric unit of the triclinic polymorph (form I: CBMZPN11), and open circles to the *C*-monoclinic polymorph (form IV: CBMZPN12). Planar  $\text{CNH}_2$  conformations lie on the black dashed line, which separates the two different pyramidalization configurations, with the top left having the hydrogen atoms pointing to the seven-membered ring.

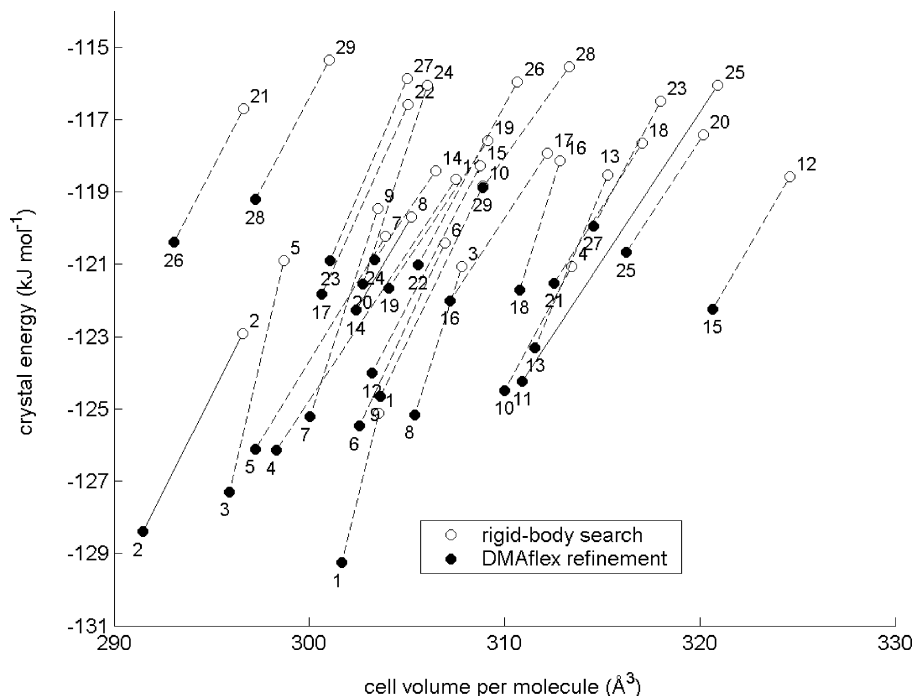
although no definite conclusions can be made because of X-ray limitations.<sup>66</sup>

The DMAflex reproduction quality for all four carbamazepine polymorphs is satisfactory (Table 3). The refined flexible torsion angles are within a few degrees of their values in the crystal and significantly different from those in the unconstrained ab initio minima (Figures 3 and 4). This suggests that these torsion angles are determined by a fine balance of intra- and intermolecular forces, which is well-described by our model. The energy reranking due to the refinement of the rigid-body search results improves the relative stability of the known structures (Figure 5). The global minimum still corresponds to a putative chain structure,<sup>26</sup> but the energy difference from the thermodynamically stable form III is reduced from 2.2 kJ mol<sup>-1</sup> to 0.9 kJ mol<sup>-1</sup>. Moreover, form IV becomes the 11th most stable structure, 5.0 kJ mol<sup>-1</sup> higher in energy than the global minimum, whereas in the rigid-body search, it was ranked 25th (9 kJ mol<sup>-1</sup> above the global minimum). The rigid-body minimizations predicted that the triclinic form I and trigonal form II had lattice energies of +7.3 and +9.7 kJ mol<sup>-1</sup>, respectively, relative to the global minimum; that is, their ranks would respectively be 18 and 30 if we assume that no other structures would be found under a more exhaustive search. When the molecular flexibility is accounted for, forms I and II become the 9th and 15th most stable structures, respectively, at +4.4 and +6.8 kJ mol<sup>-1</sup> higher in energy than the global minimum.

On the basis of differential scanning calorimetry and heat of solution measurements, it has been deduced that the most

stable polymorph is the monoclinic form III, followed by the triclinic form I (+1.34<sup>60</sup> to +3.00<sup>67</sup> kJ mol<sup>-1</sup>), the *C*-centered monoclinic IV (+1.93<sup>60</sup> kJ mol<sup>-1</sup>), and finally the loosely packed trigonal form II (+2.89<sup>60</sup> kJ mol<sup>-1</sup>). The stability order follows the density order at room temperature, which is expected given that all of the forms exhibit the same hydrogen-bonded dimers through the carboxamide donor and acceptor and differ in the way the aromatic rings interact and the pattern of weak C–H···O interactions. After the refinement, the predicted stability order of the four polymorphs is in reasonable agreement with experimental evidence (I +3.3, IV +4.17, and II +5.9 kJ mol<sup>-1</sup> with respect to form III; Table 6), although the enthalpy differences are slightly overestimated.

It is encouraging that in a few cases the flexible molecule minimization inverts the direction of the amide hydrogen atoms. The DMAflex refinement of the 25th most stable structure (which corresponds to the known form IV) alters the torsion angles  $\theta_2$  and  $\theta_3$  by 27° and 38°, respectively, with the hydrogen atoms pointing away from the ring at the minimum in good agreement with the experimental values (see Table 6 and Figure S1 of the Supporting Information). The significant adjustment of the amide hydrogen atoms construes the considerable reranking of this structure, and hence, the DMAflex refinement seems to have overcome any bias from the initial rigid-body search. Overall, after refinement, the ranges in which the torsion angles  $\theta_1$ ,  $\theta_2$ ,  $\theta_3$ , and  $\theta_4$  of the search structures vary are 22.0, 32.8, 37.7, and 12.8° and are comparable to the ranges observed for the known polymorphs and solvate crystals. The changes in lattice



**Figure 5.** Refinement (full circles) of the 29 most stable crystal structures identified by the rigid-body search (open circles, ref 26) for carbamazepine. The solid lines correspond to experimentally determined polymorphs and the dashed lines to hypothetical low-energy crystal structures.

lengths are modest and do not exceed 0.5 Å, while the average reduction in cell volume is 1.4%. In contrast with the diastereomeric salt case, the refinement does not always improve the hydrogen-bond geometry (see Table S4 in the Supporting Information), which suggests that the changes in conformation are strongly driven by the stronger dispersion arising from a denser lattice.

#### 4. Discussion

In molecular crystals, the intermolecular bonding energies are significantly weaker than the energy of typical covalent energies, and thus, the packing-induced molecular distortions are often limited.<sup>28</sup> Hence, using the *ab initio* optimized molecular structures is often a good approximation to the conformations in crystals, and crystal structure prediction studies using such molecular structures as rigid provide a good starting point.<sup>43,68,69</sup> Nevertheless, this work has demonstrated that the consideration of molecular flexibility, such as NH<sub>2</sub> geometries, within the lattice energy minimization significantly alters the ranking of the putative structures. The DMAflex approach addresses this issue by using quantum mechanical calculations to estimate the molecular deformation energy. This eliminates the inaccuracies associated with the use of empirical intramolecular potentials due to their oversimplified functional form and the fact that they have often been parametrized in conjunction with different intermolecular models than those actually used in the modeling (or even use an electrostatic model derived for intermolecular interactions to evaluate intramolecular energy contributions<sup>14,70</sup>). Moreover, DMAflex uses a realistic distributed multipole representation of the charge density for the intermolecular electrostatic contributions, to ensure that the orientation dependence of strong directional interactions,

such as hydrogen bonds and  $\pi$ - $\pi$  stacking, is modeled accurately. The conformational dependence of the charge distribution, reflecting the through-space polarization effects due to changes in the relative positions of the functional groups, is automatically accounted for by the recalculation of the distributed multipoles at each outer minimization step. The minimization of a wide set of experimentally determined crystal structures demonstrates that the approach offers substantial accuracy improvements in comparison with existing methodologies.<sup>14</sup>

Although the DMAflex methodology constitutes a significant improvement over empirical inter- and intramolecular force fields, its applicability is restricted by the computational cost and the limited degree of molecular flexibility that can be practically considered without an analytical functional form for the derivatives of the crystal energy,  $E^{\text{cryst}}$ , with respect to conformation. The need to restrict the number of conformational variables that are optimized within the crystal energy minimization is satisfied by partitioning the intramolecular degrees of freedom into rigid and flexible, which is to some extent arbitrary and relies on chemical intuition. Moreover, the computational cost is significant even when the effect of the packing forces is restricted to a limited set of easily deformable torsion angles. For example, the optimization of the salt structure illustrated in Figure 2 involved two SCF optimizations and two MP2 charge density calculations for each of the 80 outer minimization steps required to reach convergence for the four conformational variables. The computing time for a crystal energy minimization depends on the molecular size and number of conformational degrees of freedom and, for the results reported in this paper, varied from a few hours to two weeks when executed serially on a modern workstation.



**Table 6.** Effect of Conformational Relaxation on the Crystal Structure Prediction of Carbamazepine<sup>a</sup>

rigid-body search		flexible-molecule refinement							
rank, space group, graph set	$U^b$ (kJ mol <sup>-1</sup> )	rank	$\Delta E^c$	$U^d + \Delta E^c$ (kJ mol <sup>-1</sup> )	$\bar{V}^e$ (Å <sup>3</sup> )	$\theta_1$ (deg)	$\theta_2$ (deg)	$\theta_3$ (deg)	$\theta_4$ (deg)
1, <i>P2<sub>1</sub>/c</i> , C4	-125.11	1	0.169	-129.25	301.68	6.16	-171.39	-18.15	101.50
<b>2, <i>P2<sub>1</sub>/c</i>, R<sub>2</sub><sup>2</sup>(8)</b>	<b>-122.92</b>	<b>2</b>	<b>1.538</b>	<b>-128.40</b>	<b>291.48</b>	<b>-1.27</b>	<b>175.77</b>	<b>0.87</b>	<b>102.96</b>
form III						<b>(-1.64)</b>	<b>(179.54)</b>	<b>(-4.01)</b>	<b>(104.17)</b>
3, <i>P2<sub>1</sub>/c</i> , C4	-121.06	8	0.171	-125.16	305.39	5.63	-171.39	-17.67	101.97
4, <i>P2<sub>1</sub>2<sub>1</sub>2<sub>1</sub></i> , C4	-121.06	10	0.128	-124.49	309.99	1.66	-168.59	-19.94	102.65
5, <i>P1</i> , R <sub>2</sub> <sup>2</sup> (8)	-120.90	3	2.604	-127.29	295.92	4.47	173.54	13.65	104.69
6, <i>Pbca</i> , C4	-120.42	6	0.574	-125.48	302.55	6.06	-172.74	-13.00	103.16
7, <i>P1</i> , R <sub>2</sub> <sup>2</sup> (8)	-120.24	5	2.416	-126.11	297.22	10.03	-178.06	5.84	99.60
8, <i>P1</i> , R <sub>2</sub> <sup>2</sup> (8)	-119.69	14	0.220	-122.28	302.39	3.83	-165.75	-21.96	104.26
9, <i>P2<sub>1</sub>/c</i> , R <sub>2</sub> <sup>2</sup> (8)	-119.46	7	1.826	-125.21	300.05	5.43	-177.84	7.16	101.81
10, <i>P2<sub>1</sub>/c</i> , C4	-118.85	9	0.697	-124.66	303.63	5.90	-174.06	-10.98	102.77
11, <i>Pna2<sub>1</sub></i> , C2	-118.64	4	3.374	-126.14	298.32	9.98	-158.92	-22.32	109.10
12, <i>P2<sub>1</sub>/c</i> , C4	-118.58	15	0.120	-122.24	320.65	-0.13	-167.96	-20.81	105.67
13, <i>P1</i> , R <sub>2</sub> <sup>2</sup> (8)	-118.53	13	0.492	-123.30	311.56	7.88	-165.46	-20.21	98.57
14, <i>P1</i> , none	-118.42	24	0.197	-120.88	303.36	6.65	-168.04	-24.04	102.88
15, <i>P2<sub>1</sub>/c</i> , R <sub>2</sub> <sup>2</sup> (8)	-118.27	12	2.391	-124.01	303.21	8.21	-179.89	7.82	101.26
16, <i>P2<sub>1</sub>/c</i> , R <sub>2</sub> <sup>2</sup> (8)	-118.14	18	0.345	-121.71	310.77	8.57	-167.52	-20.44	97.94
17, <i>C2/c</i> , R <sub>2</sub> <sup>2</sup> (8)	-117.94	16	1.591	-122.01	307.19	-4.61	-162.75	-23.62	103.93
18, <i>P1</i> , R <sub>2</sub> <sup>2</sup> (8)	-117.66	21	0.328	-121.52	312.55	-0.23	-173.89	-17.49	106.52
19, <i>P2<sub>1</sub>/c</i> , C4	-117.59	19	0.778	-121.66	304.08	3.45	-165.09	-23.85	98.27
20, <i>P2<sub>1</sub></i> , C4	-117.43	25	0.135	-120.67	316.22	0.33	-167.75	-22.79	104.34
21, <i>P2<sub>1</sub>/c</i> , C4	-116.70	26	0.929	-120.39	293.07	-3.44	-170.52	-10.41	108.04
22, <i>P2<sub>1</sub>/c</i> , C4	-116.59	17	0.996	-121.83	300.63	6.20	-173.72	-10.73	104.88
23, <i>P2<sub>1</sub>/c</i> , R <sub>2</sub> <sup>2</sup> (8)	-116.49	27	0.241	-119.95	314.55	6.22	-166.98	-22.35	99.49
24, <i>P2<sub>1</sub>/c</i> , R <sub>2</sub> <sup>2</sup> (8)	-116.05	20	1.920	-121.55	302.73	4.82	-179.56	3.97	103.94
<b>25, <i>C2/c</i>, R<sub>2</sub><sup>2</sup>(8)</b>	<b>-116.05</b>	<b>11</b>	<b>1.820</b>	<b>-124.23</b>	<b>310.91</b>	<b>8.10</b>	<b>168.26</b>	<b>7.98</b>	<b>96.33</b>
form IV						<b>(7.50)</b>	<b>(171.51)</b>	<b>(3.00)</b>	<b>(96.62)</b>
26, <i>P2<sub>1</sub>/c</i> , R <sub>2</sub> <sup>2</sup> (8)	-115.97	22	2.550	-121.03	305.58	6.69	-178.19	5.34	104.32
27, <i>Pbca</i> , C4	-115.87	23	0.833	-120.91	301.07	-11.94	-172.71	-11.94	106.29
28, <i>Pbca</i> , C4	-115.53	29	0.216	-118.88	308.88	2.24	-166.37	-22.96	102.59
29, <i>Pna2<sub>1</sub></i> , C4	-115.35	28	0.953	-119.22	297.23	-3.02	-170.44	-10.08	106.46
Known Polymorphs out of the Scope of the Rigid-Body Search									
<b>form II</b>		<b>3.03</b>	<b>-122.49</b>	<b>314.54</b>	<b>12.04</b>	<b>179.34</b>	<b>15.77</b>	<b>95.54</b>	
					<b>(13.38)</b>			<b>(95.82)</b>	
<b>form I</b>		<b>5.04</b>	<b>-125.09</b>	<b>298.51</b>	<b>13.56</b>	<b>-175.12</b>	<b>16.51</b>	<b>97.50</b>	
					<b>(17.74)</b>	<b>(-167.15)</b>	<b>(21.74)</b>	<b>(97.23)</b>	
		<b>3.05</b>			<b>11.46</b>	<b>-178.68</b>	<b>10.94</b>	<b>98.24</b>	
					<b>(15.22)</b>	<b>(-167.20)</b>	<b>(11.28)</b>	<b>(96.05)</b>	
		<b>1.35</b>			<b>11.40</b>	<b>-173.40</b>	<b>-7.11</b>	<b>97.88</b>	
					<b>(11.79)</b>	<b>(178.98)</b>	<b>(7.03)</b>	<b>(96.66)</b>	
		<b>3.11</b>			<b>9.18</b>	<b>177.29</b>	<b>20.49</b>	<b>97.17</b>	
					<b>(15.91)</b>	<b>(-167.37)</b>	<b>(15.85)</b>	<b>(95.12)</b>	

<sup>a</sup> The rows in bold correspond to the experimentally determined forms found in the search with the experimental values of the intramolecular degrees of freedom shown in parentheses. <sup>b</sup> Intermolecular lattice energy calculated with the MP2/6-31G(d,p) global conformational minimum ( $\theta_1 = -0.46^\circ$ ,  $\theta_2 = -165.19^\circ$ ,  $\theta_3 = -29.80^\circ$ , and  $\theta_4 = 109.50^\circ$ ) and atomic multipoles derived from the MP2/6-31G(d,p) charge density with a 15 Å cutoff distance for the repulsion–dispersion and higher multipole moment interactions (ref 26). <sup>c</sup> HF/6-31G(d,p) intramolecular energy for the conformation at the crystal energy minimum. The flexible torsions at the HF/6-31G(d,p) global minimum are  $\theta_1 = 2.98^\circ$ ,  $\theta_2 = -169.85^\circ$ ,  $\theta_3 = -22.36^\circ$ , and  $\theta_4 = 103.68^\circ$ . <sup>d</sup> Intermolecular lattice energy at the crystal energy minimum with atomic multipoles derived from the MP2/6-31G(d,p) charge density and a 60 Å cutoff distance for the repulsion–dispersion and higher multipole moment interactions. <sup>e</sup> Cell volume per molecule.

The computational cost could be reduced if the rigid degrees of freedom were kept frozen to their in vacuo values  $\theta^{\text{r,vac}}$  by replacing the ab initio optimization in eq 4 with a single-point intramolecular energy evaluation:

$$\Delta E^{\text{intra}}(\theta^{\text{f}}) = E^{\text{intra}}(\theta^{\text{f}}, \theta^{\text{r,vac}}) - E^{\text{vac}} \quad (5)$$

Although this approach appears computationally attractive, we have found that it overestimates the molecular energy if the flexible degrees of freedom deviate significantly from their in vacuo values. Moreover, the ab initio optimization of the rigid degrees of freedom does not prohibitively increase the computational cost because the conformational changes are sufficiently modest so that the previously converged conformation provides an excellent starting point. A really significant decrease in computational cost could be obtained by reducing the number of iterations, and hence the number of quantum mechanical calculations, needed to reach convergence. This could be achieved by using a

gradient-based optimization algorithm, such as a Broyden–Fletcher–Goldfarb–Shanno scheme, but requires the analytical evaluation of the lattice energy gradients with respect to conformation. This preliminary study demonstrates that such an algorithm will be a significant advancement toward the reliable prediction of the structure of crystals containing flexible molecules and would also allow the estimation of realistic vibrational modes on an atomistic level and, hence, free energies. At the same time, it should also be possible to optimize all degrees of freedom within the crystal energy minimization.

The desired goal of optimization of the cell and all atomic coordinates, avoiding the inter/intra and rigid/flexible partitioning could in principle be achieved by computing the crystal energy entirely at the quantum mechanical level with periodic density functional theory. However, in addition to the prohibitive computational cost,<sup>71</sup> recent studies on the binding of molecular clusters<sup>72–74</sup> and crystals<sup>71,75</sup> questions

the ability of commonly used functionals to quantitatively predict the binding energy and geometries of dispersion-bound complexes, although empirical corrections to the van der Waals interaction energies have been recently proposed.<sup>76–78</sup> An alternative approach to avoid the use of atom–atom potentials for the intermolecular energy by relying on numerical integration over the *ab initio* charge densities<sup>79,80</sup> can, at present, only be applied for the evaluation of the lattice energy of rigid molecules. Hence, a hybrid methodology, such as DMAflex, appears to be the most currently viable approach to combine a realistic intermolecular force field with accurate models for the molecular geometry and intramolecular energy.

One problem that was overcome in the course of this study was that a few DMAflex optimizations ended in oscillations of less than 0.5 kJ mol<sup>−1</sup> in the crystal energy. This was due to discontinuities in the electrostatic interactions introduced by the distributed multipole analysis<sup>9</sup> moving the charge density contributions from the product of primitives on different atoms to the nearest nucleus. This sometimes leads to contributions to moments being switched to different nuclei when two functional groups within the molecule are in close, but changing, proximity, as with the amino and hydroxyl groups in NOREPH01. The use of a recently proposed revised multipole analysis,<sup>10</sup> which uses numerical integration for the diffuse functions, solves this problem and was used for the structure reproductions of the structures ATUVIU, NOREPH01, GAHP10, ACYGLY11, IBPRAC01, and JEKNOC11.

The importance of DMAflex refinements of crystal structures comes from their ability to reproduce the molecular deformations that lead to energetically more favorable hydrogen-bonding geometries and denser lattices than can be achieved using a rigid molecular geometry. However, it is essentially a local minimization method, and hence, it will only provide the minimum closest to the starting crystal structure. For significantly flexible systems, all low-energy minima need to be approximately located prior to refinement by using empirical force fields<sup>23</sup> or a set of rigid-body geometries,<sup>68</sup> whose number depends on the complexity of the intramolecular and crystal energy surfaces. In the case of carbamazepine, the refinement gave structures spanning the low-energy conformational space (Table 6) starting from just the *ab initio* optimized minimum. This would clearly not be sufficient to predict the conformational polymorphism of piracetam,<sup>68</sup> though the successful blind prediction of form IV could have been achieved with far fewer rigid-body searches had DMAflex refinement been used. The complexity of the  $E^{\text{cryst}}$  landscape in the case of the diastereomeric salt pair system suggests that more rigid-body searches and more DMAflex refinements over a wider energy range might well find additional structures that are energetically competitive with the known forms.

The realistic modeling of the molecular deformation under the crystalline forces constitutes an important development toward the reliable prediction of the thermodynamic stability of putative and known crystal structures. However, further improvements are necessary for the reliable prediction of thermodynamic stability: free energy differences of 3–4 kJ

mol<sup>−1</sup> correspond to a solubility ratio of 2:1, and so, such accuracy is needed for the theoretical screening of resolving agents. Although the stability order of the carbamazepine polymorphs is correctly reproduced, the global minimum still corresponds to a catemeric structure whose existence has not been experimentally confirmed despite the strenuous experimental screening.<sup>26</sup> We are currently investigating whether the development of *ab initio* repulsion–dispersion intermolecular potentials and the modeling of the polarization of the molecular charge density by the crystalline environment are likely to change the ranking of low-energy crystal structures even further. Further research is also needed in evaluating the accuracy of quantum mechanical estimates for the intramolecular energy, because of intramolecular basis set superposition errors and an inaccurate description of the dispersion interactions between distant functional groups.<sup>44</sup> For flexible systems, there is an even greater challenge in using sufficiently accurate energy models for realistic estimates of the entropic and zero-point energy contributions on one hand and thermal expansion on the other. However, the accurate modeling of the free energy alone is not likely to be sufficient for the successful prediction of the organic solid state, as concomitant polymorphism<sup>81</sup> shows that crystallization is not always thermodynamically controlled. Nevertheless, the exact extent to which kinetic effects can determine the crystallization outcome cannot be assessed without accurate thermodynamic models that reliably rank theoretically derived structures and limit the subset of these that should be considered as potential polymorphs.<sup>13,24,78</sup>

## 5. Conclusions

This paper presents a novel methodology for the lattice energy minimization of crystal structures which contain molecular entities whose conformation may be distorted under the packing forces. The proposed approach aims to address the limitations of rigid-body minimizations when the lattice energy is particularly sensitive to the molecular conformations, as is often the case in the modeling of strongly bound hydrogen-bonded crystals, such as salts.<sup>25</sup> The minimization of a wide set of experimentally determined crystal structures and the reminimization of putative structures earlier generated by rigid-body searches demonstrate that the approach offers substantial accuracy improvements in comparison to existing methodologies.

**Acknowledgment.** The authors acknowledge financial support from the Basic Technology Program of the Research Councils U. K. as part of the CPOSS project (<http://www.cposs.org.uk>) and are grateful for the use of UCL Research Computing services (C<sup>3</sup>).

**Supporting Information Available:** Details regarding the reproduction of the experimentally determined 1-phenylethylammonium 2-phenylpropanoate crystal structures (Table S1), the changes in cell and hydrogen-bond geometries during the DMAflex refinement of the most stable 1-phenylethylammonium 2-phenylpropanoate (Tables S2 and S3) and carbamazepine (Table S4) rigid-body minima, and the overlay of the experimental and rigid-body (Figure S1a) and

flexible molecule (Figure S1b) minima for form IV of carbamazepine. This information is available free of charge via the Internet at <http://pubs.acs.org>.

### References

- (1) Verwer, P.; Leusen, F. J. J. Computer Simulation to Predict Possible Crystal Polymorphs. In *Reviews in Computational Chemistry*; Lipkowitz, K. B., Boyd, D. B., Eds.; Wiley-VCH: New York, 1998; pp 327–365.
- (2) Lommerse, J. P. M.; Motherwell, W. D. S.; Ammon, H. L.; Dunitz, J. D.; Gavezzotti, A.; Hofmann, D. W. M.; Leusen, F. J. J.; Mooij, W. T. M.; Price, S. L.; Schweizer, B.; Schmidt, M. U.; Van Eijck, B. P.; Verwer, P.; Williams, D. E. *Acta Crystallogr., Sect. B* **2000**, *56*, 697–714.
- (3) Motherwell, W. D. S.; Ammon, H. L.; Dunitz, J. D.; Dzyabchenko, A.; Erk, P.; Gavezzotti, A.; Hofmann, D. W. M.; Leusen, F. J. J.; Lommerse, J. P. M.; Mooij, W. T. M.; Price, S. L.; Scheraga, H.; Schweizer, B.; Schmidt, M. U.; Van Eijck, B. P.; Verwer, P.; Williams, D. E. *Acta Crystallogr., Sect. B* **2002**, *58*, 647–661.
- (4) Day, G. M.; Motherwell, W. D. S.; Ammon, H. L.; Boerrigter, S. X. M.; Della Valle, R. G.; Venuti, E.; Dzyabchenko, A.; Dunitz, J. D.; Schweizer, B.; Van Eijck, B. P.; Erk, P.; Facelli, J. C.; Bazterra, V. E.; Ferraro, M. B.; Hofmann, D. W. M.; Leusen, F. J. J.; Liang, C.; Pantelides, C. C.; Karamertzanis, P. G.; Price, S. L.; Lewis, T. C.; Nowell, H.; Torrisi, A.; Scheraga, H. A.; Arnautova, Y. A.; Schmidt, M. U.; Verwer, P. *Acta Crystallogr., Sect. B* **2005**, *61*, 511–527.
- (5) Van Eijck, B. P.; Kroon, J. *Acta Crystallogr., Sect. B* **2000**, *56*, 535–542.
- (6) Van Eijck, B. P. *J. Comput. Chem.* **2002**, *23*, 456–462.
- (7) Dunitz, J. D.; Scheraga, H. A. *PNAS* **2004**, *101*, 14309–14311.
- (8) Van Eijck, B. P. *Acta Crystallogr., Sect. B* **2005**, *61*, 528–535.
- (9) Stone, A. J.; Alderton, M. *Mol. Phys.* **1985**, *56*, 1047–1064.
- (10) Stone, A. J. *J. Chem. Theory Comput.* **2005**, *1*, 1128–1132.
- (11) Price, S. L. *J. Chem. Soc., Faraday Trans.* **1996**, *92*, 2997–3008.
- (12) Coombes, D. S.; Price, S. L.; Willock, D. J.; Leslie, M. J. *Phys. Chem.* **1996**, *100*, 7352–7360.
- (13) Day, G. M.; Motherwell, W. D. S.; Jones, W. *Cryst. Growth Des.* **2005**, *5*, 1023–1033.
- (14) Brodersen, S.; Wilke, S.; Leusen, F. J. J.; Engel, G. *Phys. Chem. Chem. Phys.* **2003**, *5*, 4923–4931.
- (15) Mooij, W. T. M. Ab Initio Prediction of Crystal Structures. Ph.D. Thesis, Utrecht University, Utrecht, The Netherlands, 2000.
- (16) Gavezzotti, A. *Modell. Simul. Mater. Sci. Eng.* **2002**, *10*, R1–R29.
- (17) Koch, U.; Popelier, P. L. A.; Stone, A. J. *Chem. Phys. Lett.* **1995**, *238*, 253–260.
- (18) Price, S. L. *J. Chem. Soc., Faraday Trans.* **1992**, *88*, 1755–1763.
- (19) Dudek, M. J.; Ponder, J. W. *J. Comput. Chem.* **1995**, *16*, 791–816.
- (20) Koch, U.; Stone, A. J. *J. Chem. Soc., Faraday Trans.* **1996**, *92*, 1701–1708.
- (21) Mooij, W. T. M.; Van Eijck, B. P.; Kroon, J. *J. Phys. Chem. A* **1999**, *103*, 9883–9890.
- (22) Mooij, W. T. M.; Van Eijck, B. P.; Kroon, J. *J. Am. Chem. Soc.* **2000**, *122*, 3500–3505.
- (23) Van Eijck, B. P.; Mooij, W. T. M.; Kroon, J. *J. Comput. Chem.* **2001**, *22*, 805–815.
- (24) Van Eijck, B. P.; Mooij, W. T. M.; Kroon, J. *J. Phys. Chem. B* **2001**, *105*, 10573–10578.
- (25) Karamertzanis, P. G.; Price, S. L. *J. Phys. Chem. B* **2005**, *109*, 17134–17150.
- (26) Florence, A. J.; Johnston, A.; Price, S. L.; Nowell, H.; Kennedy, A. R.; Shankland, N. *J. Pharm. Sci.* **2006**, in press.
- (27) Willock, D. J.; Price, S. L.; Leslie, M.; Catlow, C. R. A. *J. Comput. Chem.* **1995**, *16*, 628–647.
- (28) Allen, F. H.; Harris, S. E.; Taylor, R. *J. Comput.-Aided Mol. Des.* **1996**, *10*, 247–254.
- (29) Osborn, J. C.; York, P. *J. Mol. Struct.* **1999**, *474*, 43–47.
- (30) Pertsin, A. J.; Kitaigorodsky, A. I. *The Atom-Atom Potential Method. Applications to Organic Molecular Solids*; Springer-Verlag: Berlin, 1987.
- (31) Gavezzotti, A. Crystal Symmetry and Molecular Recognition. In *Theoretical Aspects and Computer Modeling of the Molecular Solid State*; Gavezzotti, A., Ed.; John Wiley & Sons: Chichester, U. K., 1997.
- (32) Stone, A. J. *Chem. Phys. Lett.* **1981**, *83*, 233–239.
- (33) Cox, S. R.; Hsu, L. Y.; Williams, D. E. *Acta Crystallogr., Sect. A* **1981**, *37*, 293–301.
- (34) Williams, D. E.; Cox, S. R. *Acta Crystallogr., Sect. B* **1984**, *40*, 404–417.
- (35) Williams, D. E.; Houpt, D. J. *Acta Crystallogr., Sect. B* **1986**, *42*, 286–295.
- (36) Ewald, P. *Ann. Phys.* **1921**, *64*, 253.
- (37) Leslie, M. *Mol. Phys.* **2006**, in press.
- (38) Nelder, J. A.; Mead, R. *Comput. J.* **1965**, *7*, 308–313. Implemented in Numerical Recipes (<http://www.numerical-recipes.com>; accessed May 2006).
- (39) Frisch, M. J.; Trucks, G. W.; Schlegel, H. B.; Scuseria, G. E.; Robb, M. A.; Cheeseman, J. R.; Zakrzewski, V. G.; Montgomery, J. A., Jr.; Stratmann, R. E.; Burant, J. C.; Dapprich, S.; Millam, J. M.; Daniels, A. D.; Kudin, K. N.; Strain, M. C.; Farkas, O.; Tomasi, J.; Barone, V.; Cossi, M.; Cammi, R.; Mennucci, B.; Pomelli, C.; Adamo, C.; Clifford, S.; Ochterski, J.; Petersson, G. A.; Ayala, P. Y.; Cui, Q.; Morokuma, K.; Malick, D. K.; Rabuck, A. D.; Raghavachari, K.; Foresman, J. B.; Cioslowski, J.; Ortiz, J. V.; Stefanov, B. B.; Liu, G.; Liashenko, A.; Piskorz, P.; Komaromi, I.; Gomperts, R.; Martin, R. L.; Fox, D. J.; Keith, T.; Al-Laham, M. A.; Peng, C. Y.; Nanayakkara, A.; Gonzalez, C.; Challacombe, M.; Gill, P. M. W.; Johnson, B. G.; Chen, W.; Wong, M. W.; Andres, J. L.; Head-Gordon, M.; Replogle, E. S.; Pople, J. A. *Gaussian 98*, revision A.9; Gaussian, Inc.: Pittsburgh, PA, 1998.
- (40) Allen, F. H. *Acta Crystallogr., Sect. B* **2002**, *58*, 380–388.
- (41) Chisholm, J. A.; Motherwell, S. *J. Appl. Crystallogr.* **2005**, *38*, 228–231.
- (42) Allen, F. H.; Kennard, O.; Watson, D. G. *J. Chem. Soc., Perkin Trans. 2* **1987**, S1–S19.

- (43) Price, S. L. *Adv. Drug Delivery Rev.* **2004**, *56*, 301–319.
- (44) van Mourik, T.; Karamertzanis, P. G.; Price, S. L. *J. Phys. Chem. A* **2006**, *110*, 8–12.
- (45) Vishweshwar, P.; McMahon, J. A.; Oliveira, M.; Peterson, M. L.; Zaworotko, M. J. *J. Am. Chem. Soc.* **2005**, *127*, 16802–16803.
- (46) Bernstein, J. *Polymorphism in Molecular Crystals*; Oxford Science Publications: Oxford, U. K., 2002.
- (47) Rekoske, J. E. *AIChE J.* **2001**, *47*, 2.
- (48) Jacques, J.; Collet, A.; Wilen, S. H. *Enantiomers, Racemates and Resolutions*; Wiley-Interscience: New York, 1981.
- (49) Pasteur, L. C. R. *Hebdomadae Seances Acad. Sci.* **1853**, *37*, 162.
- (50) Karamertzanis, P. G.; Hulme, A. T.; Anandamanoharan, P. R.; Cains, P. W.; Vickers, M.; Tocher, D. A. **2006**, in preparation.
- (51) Dufour, F.; Perez, G.; Coquerel, G. *Bull. Chem. Soc. Jpn.* **2004**, *77*, 79–86.
- (52) Taylor, R.; Kennard, O.; Versichel, W. *J. Am. Chem. Soc.* **1983**, *105*, 5761–5766.
- (53) Taylor, R.; Kennard, O.; Versichel, W. *Acta Crystallogr., Sect. B* **1984**, *40*, 280–288.
- (54) Taylor, R.; Kennard, O. *Acc. Chem. Res.* **1984**, *17*, 320–326.
- (55) Taylor, R.; Kennard, O. *Acta Crystallogr., Sect. B* **1983**, *39*, 133–138.
- (56) Lowes, M. M. J.; Caira, M. R.; Lotter, A. P.; van der Watt, J. G. *J. Pharm. Sci.* **1987**, *76*, 744–752.
- (57) Himes, V. L.; Mighell, A. D.; DeCamp, W. H. *Acta Crystallogr., Sect. B* **1981**, *37*, 2242–2245.
- (58) Rustichelli, C.; Gamberini, G.; Ferioli, V.; Gamberini, M. C.; Ficarra, R.; Tommasini, S. *J. Pharm. Biomed. Anal.* **2000**, *23*, 41–54.
- (59) Lang, M. D.; Kampf, J. W.; Matzger, A. J. *J. Pharm. Sci.* **2002**, *91*, 1186–1190.
- (60) Grzesiak, A. L.; Lang, M. D.; Kim, K.; Matzger, A. J. *J. Pharm. Sci.* **2003**, *92*, 2260–2271.
- (61) Fleischman, S. G.; Kuduva, S. S.; McMahon, J. A.; Moulton, B.; Walsh, R. D. B.; Rodriguez-Hornedo, N.; Zaworotko, M. J. *Cryst. Growth Des.* **2003**, *3*, 909–919.
- (62) Lang, M. D.; Grzesiak, A. L.; Matzger, A. J. *J. Am. Chem. Soc.* **2002**, *124*, 14834–14835.
- (63) Hilfiker, R.; Berghausen, J.; Blatter, F.; Burkhard, A.; De Paul, S. M.; Freiermuth, B.; Geoffroy, A.; Hofmeier, U.; Marcolli, C.; Siebenhaar, B.; Szelagiewicz, M.; Vit, A.; von Raumer, M. *J. Therm. Anal. Calorim.* **2003**, *73*, 429–440.
- (64) Strachan, C. J.; Howell, S. L.; Rades, T.; Gordon, K. C. *J. Raman Spectrosc.* **2004**, *35*, 401–408.
- (65) Cruz-Cabera, A. J.; Day, G. M.; Motherwell, W. D. S.; Jones, W. *Cryst. Growth Des.* **2006**, in press.
- (66) Speakman, J. C. In *Molecular Structure by Diffraction Methods*; Sim, G. A., Sutton, L. E., Eds.; The Chemical Society: London, 1973; p 203.
- (67) Chong-Hui, G.; Grant, D. J. W. *J. Pharm. Sci.* **2001**, *90*, 1277–1287.
- (68) Nowell, H.; Price, S. L. *Acta Crystallogr., Sect. B* **2005**, *61*, 558–568.
- (69) Ouvrard, C.; Price, S. L. *Cryst. Growth Des.* **2004**, *4*, 1119–1127.
- (70) Mooij, W. T. M.; Leusen, F. J. J. *Phys. Chem. Chem. Phys.* **2001**, *3*, 5063–5066.
- (71) Chisholm, J. A.; Motherwell, S.; Tulip, P. R.; Parsons, S.; Clark, S. J. *Cryst. Growth Des.* **2005**, *5*, 1437–1442.
- (72) van Mourik, T.; Gdanitz, R. J. *J. Chem. Phys.* **2002**, *116*, 9620–9623.
- (73) Tsuzuki, S.; Luthi, H. P. *J. Chem. Phys.* **2001**, *114*, 3949–3957.
- (74) Johnson, E. R.; Wolkow, R. A.; DiLabio, G. A. *Chem. Phys. Lett.* **2004**, *394*, 334–338.
- (75) Montanari, B.; Ballone, P.; Jones, R. O. *J. Chem. Phys.* **1998**, *108*, 6947–6951.
- (76) Elstner, M.; Hobza, P.; Frauenheim, T.; Suhai, S.; Kaxiras, E. *J. Chem. Phys.* **2001**, *114*, 5149–5155.
- (77) Wu, Q.; Yang, W. T. *J. Chem. Phys.* **2002**, *116*, 515–524.
- (78) Neumann, M. A.; Perrin, M. A. *J. Phys. Chem. B* **2005**, *109*, 15531–15541.
- (79) Gavezzotti, A. *J. Phys. Chem. B* **2002**, *106*, 4145–4154.
- (80) Gavezzotti, A. *J. Phys. Chem. B* **2003**, *107*, 2344–2353.
- (81) Bernstein, J.; Davey, R. J.; Henck, J. O. *Angew. Chem., Int. Ed.* **1999**, *38*, 3441–3461.

CT600111S